Article

http://dx.doi.org/10.20517/element.2026.05

Hepatic Smad4 mediates antibacterial defense via macrophage recruitment

Liyun Chen, Wenxi Zhao, Qian Wu, Chaohui Lin, Rong Wang, Zijun Song, Hongbing Luo, Yingying Yu, Günter Weiss, Junxia Min, Fudi Wang

Graphical abstract

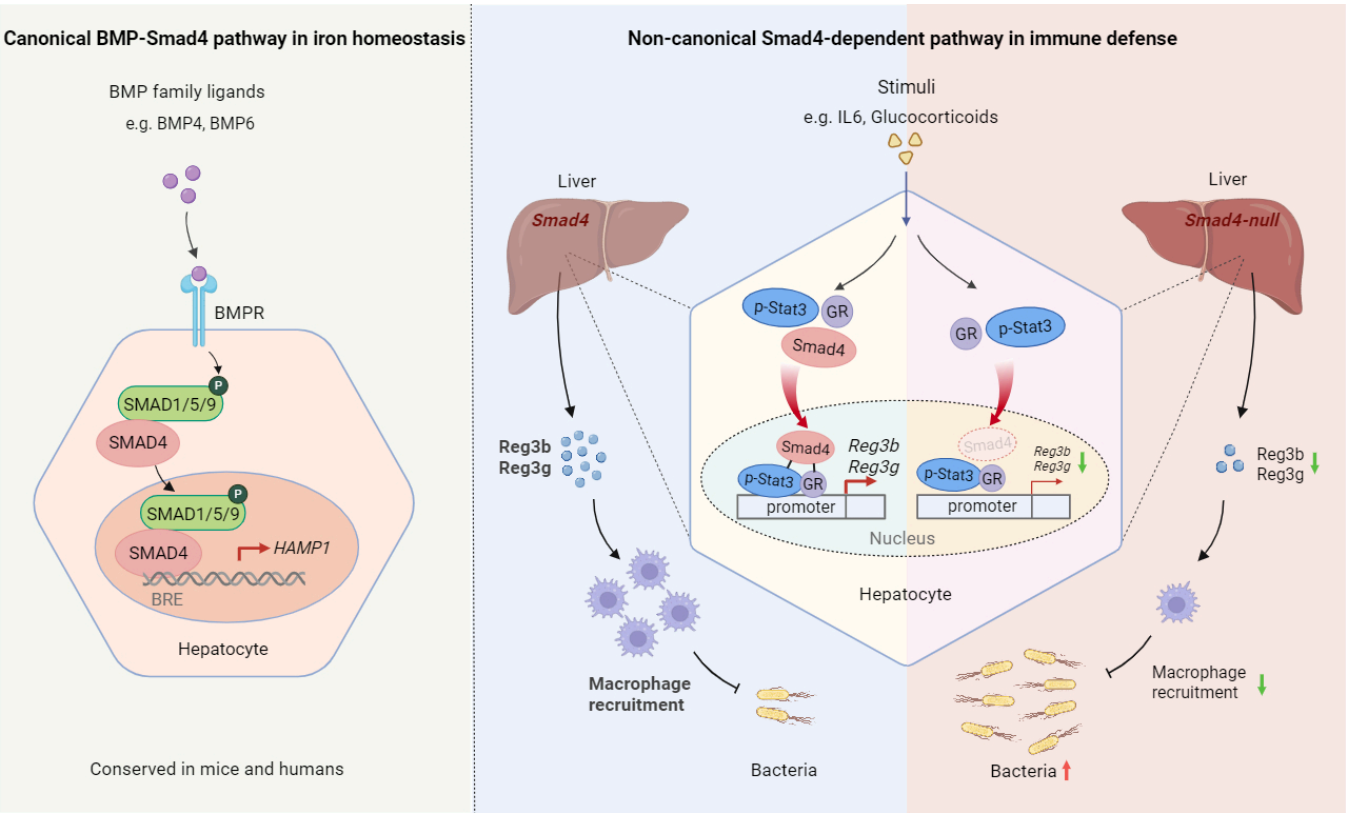

Highlights

- Smad4 mediates immune defense via a non-canonical pathway distinct from its BMP-linked iron regulation.
- Hepatic Smad4 acts as a co-activator for Stat3 and glucocorticoid receptor to drive Reg3b and Reg3g transcription.
- Hepatocyte-derived Reg3b and Reg3g contribute to macrophage migration during bacterial infection.
- Restoring systemic iron balance with diet cannot reverse infection vulnerability in Smad4-deficient mice.

Article

http://dx.doi.org/10.20517/element.2026.05

Hepatic Smad4 mediates antibacterial defense via macrophage recruitment

Liyun Chen[1,2,#], Wenxi Zhao[1,#], Qian Wu[3,#], Chaohui Lin[1], Rong Wang[1], Zijun Song[1], Hongbing Luo[1], Yingying Yu[4], Günter Weiss[5] ✉, Junxia Min[2] ✉, Fudi Wang[1] ✉

Received: 11 Feb 2026
Accepted: 30 Jun 2026
Online: 6 Aug 2026
Open Access

ABSTRACT

Host defense against bacterial infection requires precise organ-immune coordination, but the hepatic regulatory mechanisms remain unclear. As a key factor of the hepatic transforming growth factor-beta (TGF-β) signaling pathway, Smad4 is well known for its roles in iron metabolism and tissue repair, yet its function in hepatic antimicrobial immunity is poorly defined. Using hepatocyte-specific Smad4 knockout mice (LKO), we found Smad4 is essential for survival upon *Escherichia coli or Staphylococcus aureus* infection. LKO mice showed higher bacterial burden, liver injury, and reduced macrophage recruitment - phenotypes that were non-iron dependent. Transcriptomic and functional studies identified *Reg3b/Reg3g* as key Smad4 targets mediating macrophage recruitment. Recombinant *Reg3b/3g* rescued infection outcomes in LKO mice. Mechanistically, Smad4 acts as a co-activator, promoting Stat3 and glucocorticoid receptor (GR) binding to *Reg3b/3g* promoters, thereby driving their expression. Disruption of Stat3 or GR signaling recapitulated the LKO phenotype. Our findings reveal a novel non-canonical, non-iron dependent role for hepatic Smad4 in orchestrating antibacterial defense via *Reg3b/3g*-mediated macrophage recruitment, highlighting the liver's central role in infection immunity.

Keywords: Smad4 liver antibacterial defense macrophage recruitment *Reg3b/Reg3g* iron metabolism

INTRODUCTION

Sepsis represents a critical systemic inflammatory condition triggered by an aberrant host reaction following infection, leading to profound severe organ failure along with elevated death rates worldwide[1,2]. Its pathogenesis encompasses multifaceted derangements, such as disturbances in proinflammatory cascades, mitochondrial injury, immunological defects and other processes, yet the precise cellular and molecular mechanisms that drive this syndrome remain incompletely understood[3-5].

The immune system and parenchymal organs cooperate to eliminate invading pathogens and maintain system homeostasis. In particular, the liver is increasingly recognized not only for its metabolic functions but also as a pivotal immune organ, owing to its substantial population of resident immune cells within the non-parenchymal compartment[6,7]. Kupffer cells, natural killer T cells and other various immune cell subsets are reported to function in fighting against pathogens and contribute to antibacterial defense[8-11]. Moreover, hepatocytes - the predominant cell type in the liver - also exert considerable immunoregulatory effects. In response to inflammation, hepatocytes synthesize acute phase proteins (APPs), including complements, secreted pattern-recognition receptors (PRRs) and other mediators to help counteract the possible existence of pathogens[12-15]. They also produce adhesion molecules [e.g., intercellular adhesion molecule-1 (ICAM-1)] and chemokines [e.g., interleukin-8 (IL-8), C-X-C motif chemokine ligand 1 (CXCL1)] that facilitate immune cell recruitment and adhesion[16-18]. Additionally, cytokine-induced reactive oxygen intermediates generated in

[1]The Second Affiliated Hospital, School of Public Health, State Key Laboratory of Experimental Hematology, Zhejiang University School of Medicine, Hangzhou 310058, Zhejiang, China. [2]The First Affiliated Hospital, Institute of Translational Medicine, Zhejiang University School of Medicine, Hangzhou 310058, Zhejiang, China. [3]Global Innovation Institute of Element Science (GIIES-JLU), The First Hospital of Jilin University, Changchun 130021, Jilin, China. [4]School of Public Health, Hangzhou Normal University, Hangzhou 310058, Zhejiang, China. [5]Department of Internal Medicine II, Medical University Innsbruck, Innsbruck 6020, Austria. [#]These authors contributed equally to this work.
*Correspondence to: Prof. Günter Weiss, E-mail: guenter.weiss@i-med.ac.at; Prof. Junxia Min, E-mail: junxiamin@zju.edu.cn; Prof. Fudi Wang (Lead contact), E-mail: fwang@zju.edu.cn

hepatocytes also contribute to antimicrobial activity[19]. Due to the large diversity of APPs and complex immune network governed by the liver, the hepatic regulatory mechanisms during the infection process remain incompletely elucidated.

The host defense against bacterial infection relies on multiple signaling pathways. Among them, transforming growth factor-beta (TGF-β)/Smad pathway is well recognized as a core regulatory cascade for tissue repair and anti-inflammatory responses[20]. Smad4 serves as the common-mediator of TGF-β superfamily signaling and helps regulate the development, activation, proliferation and differentiation of diverse immune cells[21], thereby preserving homeostasis of immune system. It is reported that Smad3/Smad4 in B cells synergistically promote the expression of immunoglobulin A (IgA) mediated by TGF-β1 upon lipopolysaccharide (LPS) treatment[22]. Within the myeloid lineage, Smad4 is responsible for the induction of interleukin-1 receptor-associated kinase-M (IRAK-M) and Src homology 2-containing inositol phosphatase 1 (SHIP1), the negative regulators of toll-like receptor (TLR) signaling, which contributes to endotoxin tolerance[23]. Independently of TGF-β signaling, Smad4 deficiency in T cells promotes Th2 and Th17 differentiation, which lead to the development of gastrointestinal cancer[24,25], and may also exacerbate intestinal inflammation via enhanced $CD8^+$ T cell accumulation[26]. In the liver, Smad4 is found to maintain basal transcription of iron hormone-hepcidin[27]. Accordingly, hepatocytes-specific Smad4 depletion led to systemic iron accumulation in mice. However, the immune implications of hepatocytes-specific Smad4 depletion have yet to be defined.

In the current study, we employed a bacterial infection model in hepatocytes-specific Smad4 knockout mice (LKO) and observed that these mice exhibit heightened susceptibility to bacterial infection. Through high throughput RNA sequencing, we identified *Reg3b* and *Reg3g* as the key dysregulated APPs in the liver of LKO mice which probably accounts for their immune deficient phenotype. Thus, we discovered Smad4-*Reg3b*/*Reg3g* axis in the liver as a crucial pathway for maintaining macrophage recruitment during bacterial infection. Our results revealed a novel and critical role of hepatic Smad4 in host defense.

RESULTS

Hepatocytes specific Smad4 knockout mice exhibited increased susceptibility to bacterial infection

We focused on Smad4, the key signal transducer of TGF-β pathway, and generated hepatocyte-specific Smad4 knockout mice using Albumin-Cre (hereafter LKO). To characterize the role of hepatocyte Smad4 during infection, we challenged LKO mice and wild-type controls with lethal dose of *Escherichia coli* (*E. coli*) or *Staphylococcus aureus* (*S. aureus*) intraperitoneally. The LKO mice exhibited significantly increased sensitivity to bacterial infection compared with wildtype control in both models [Figure 1A and B]. We subsequently utilized *E. coli* infection model for further investigation due to its relative biosafety. In this experimental model, all the LKO mice expired within 36 h post infection [Figure 1A]. The analysis of cytokines revealed that the level of tumor necrosis factor-alpha (TNF-α) showed no significant difference in the serum of LKO mice compared to that of control, while the level of interleukin-6 (IL-6) was slightly elevated [Figure 1C]. The mRNA expression levels of these genes were also comparable or slightly increased in the liver of LKO mice post infection [Extended Support Figure 1A]. Additionally, we observed significantly higher bacterial burden in the liver [Figure 1D], peritoneal lavage (PL), and blood [Figure 1E] of LKO mice, indicating that bacterial clearance was impaired in LKO mice. Moreover, hematoxylin and eosin (HE) staining showed enhanced erythrocyte retention in liver of LKO mice [Figure 1F], indicating the increase of vascular permeability, which is one of the typical characteristics of sepsis[28]. Finally, the LKO mice sustained greater infection-induced liver injury, as demonstrated by significantly elevated serum levels of serum ALT (alanine aminotransferase) and AST (aspartate aminotransferase) compared to control mice [Figure 1G].

Iron overload was not the major factor for susceptibility of LKO mice

Given the established role of iron metabolism in bacterial infection, we investigated its potential contribution to the phenotype observed in LKO mice. As previously reported, the LKO mice exhibit massive iron overload in the liver and circulation, attributable to low hepcidin levels [Extended Support Figure 1B and C]. Hence, we fed LKO mice with iron deficient diet (hereafter LKO-IDD) for 4 weeks to decrease their liver and serum iron to the similar level with control littermates [Extended Support Figure 1B]. Despite iron normalization, lethal dose *E. coli* challenged LKO-IDD mice still exhibited higher mortality compared to Ctrl mice [Figure 1H]. Additionally, the bacterial burden in the liver and peritoneal cavity of LKO-IDD mice remained significantly elevated than Ctrl mice [Figure 1I]. Moreover, these mice displayed significant elevations in serum ALT and AST levels. Figure 1J, indicating more severe liver injury, which was further corroborated by histopathological analysis [Extended Support Figure 1C]. Collectively, these results indicate that rectifying iron overload is insufficient to rescue the infection phenotype, suggesting that dysregulated iron metabolism is not the major cause of the heightened susceptibility to *E. coli* infection in LKO mice.

Hepatic Smad4 deletion results in decreased expression of *Reg3b* and *Reg3g* in hepatocytes

Given that the depletion of smad4 abrogated TGF-β/Bmp signaling and may lead to widespread transcriptional dysregulation, we employed RNA-seq analysis on livers from *E. coli*-infected LKO and control mice to identify key target genes. We identified 1,622 differentially expressed genes (DEGs) that were downregulated in the infected LKO mice *vs.* infected control mice [Figure 2A]. The Kyoto Encyclopedia of Genes and Genomes (KEGG) pathway analysis revealed the inflammatory response pathway was among the most significantly affected in LKO liver [Figure 2B]. Through volcano plot, we found two inflammatory-related gene, *Reg3b* and *Reg3g*, were ranked among the most strongly suppressed genes in in LKO liver upon infection [Figure 2C]. Notably, these two genes were also annotated in the inflammatory response pathway [Figure 2D].

For further insight, we also compared transcriptomes of the livers from *E. coli*-infected control mice *vs.* phosphate buffered saline (PBS)-treated controls, which revealed 2,491 DEGs that were upregulated in the group infected with *E. coli*. Furthermore, the Gene Ontology (GO) analysis of these upregulated DEGs revealed that the inflammatory response and acute-phase response pathway were significantly enhanced within the *E. coli*-infected control group [Extended Support Figure 2A]. Interestingly, *Reg3b* and *Reg3g* were among the most strongly induced genes in this dataset [Extended Support Figure 2B and C]. Comparative analysis between the two RNA-seq experiments indicated that altogether 319 genes were observed to be downregulated in infected LKO mice (*vs.* infected control mice) while upregulated in *E. coli*-control (*vs.* PBS-control mice), including *Reg3b* and *Reg3g* [Extended Support Figure 2D]. Collectively, these data demonstrate that hepatic Smad4 is indispensable for the transcriptional induction of a subset of infection responsive genes including *Reg3b* and *Reg3g* upon bacterial infection.

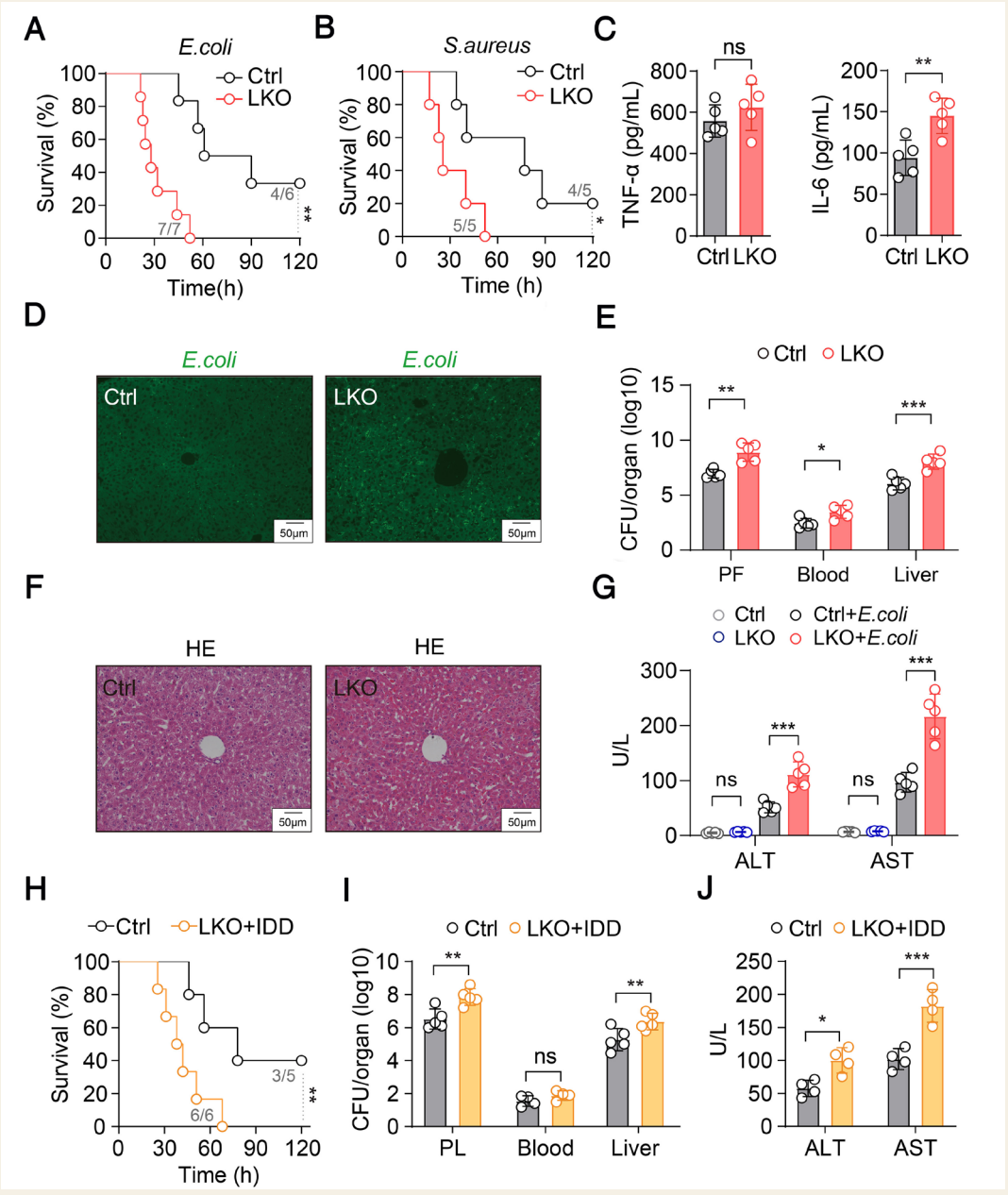

Figure 1. Hepatocytes specific Smad4 knockout mice were susceptible to bacterial infection.
(A) Kaplan-Meier survival curve of *Smad4*$^{fl/fl}$; Alb-cre (LKO) mice (n = 7) and respective controls mice (n = 6) following an i.p. injection of *E. coli*; (B) Kaplan-Meier survival curve of *Smad4*$^{fl/fl}$; Alb-cre (LKO) mice (n = 5) and respective controls mice (n = 5) following an i.p. injection of *S. aureus*; (C) The serum levels of TNF-α and IL-6 in the control and LKO mice were measured post *E. coli* infection by ELISA (n = 5 per group); (D) Fluorescence microscopy and respective quantification of liver tissues of control and LKO mice infected with GFP-labeled *E. coli*; (E) Bacterial CFU counts were measured in the peritoneal fluid, blood and liver of control (n = 5) and LKO mice (n = 5) 12 h after an i.p. injection of *E. coli*; (F) Representative hematoxylin and eosin staining of histological sections of liver tissue in control and LKO mice 12 h postinfection; (G) Serum ALT and AST levels of control (n = 5) and LKO mice (n = 5) were measured 12 h postinfection; (H) Kaplan-Meier survival curve of IDD *Smad4*$^{fl/fl}$; Alb-cre (LKO) mice (n = 6) and respective controls mice (n = 5) following an i.p. injection of *E. coli*; (I) Bacterial CFU counts were measured in the peritoneal fluid, blood and liver of control (n = 5) and IDD-LKO mice (n = 5) 12 h after an i.p. injection of *E. coli*; (J) Serum ALT and AST levels of control (n = 4) and IDD-LKO mice (n = 4) were measured 12 h postinfection. Circles correspond to individual mouse. Results are represented as mean ± SD. P values in (A, B and H) were determined using log-rank (Mantel-Cox) test. The P values in (C, E, I and J) were determined using unpaired Student's t-tests. The P values in (G) were determined using two-way ANOVA. *P < 0.05; **P < 0.01; ***P < 0.001. NS: Not significant; *E. coli*: *Escherichia coli*; *S. aureus*: *Staphylococcus aureus*; LKO: liver-specific Smad4 knockout; TNF-α: tumor necrosis factor alpha; IL-6: interleukin-6; ELISA: Enzyme-Linked Immunosorbent Assay; GFP: green fluorescent protein; CFU: colony forming unit; HE: hematoxylin and eosin; PL: peritoneal lavage; ALT: alanine transaminase; AST: aspartate transaminase; IDD: iron-deficient diet.

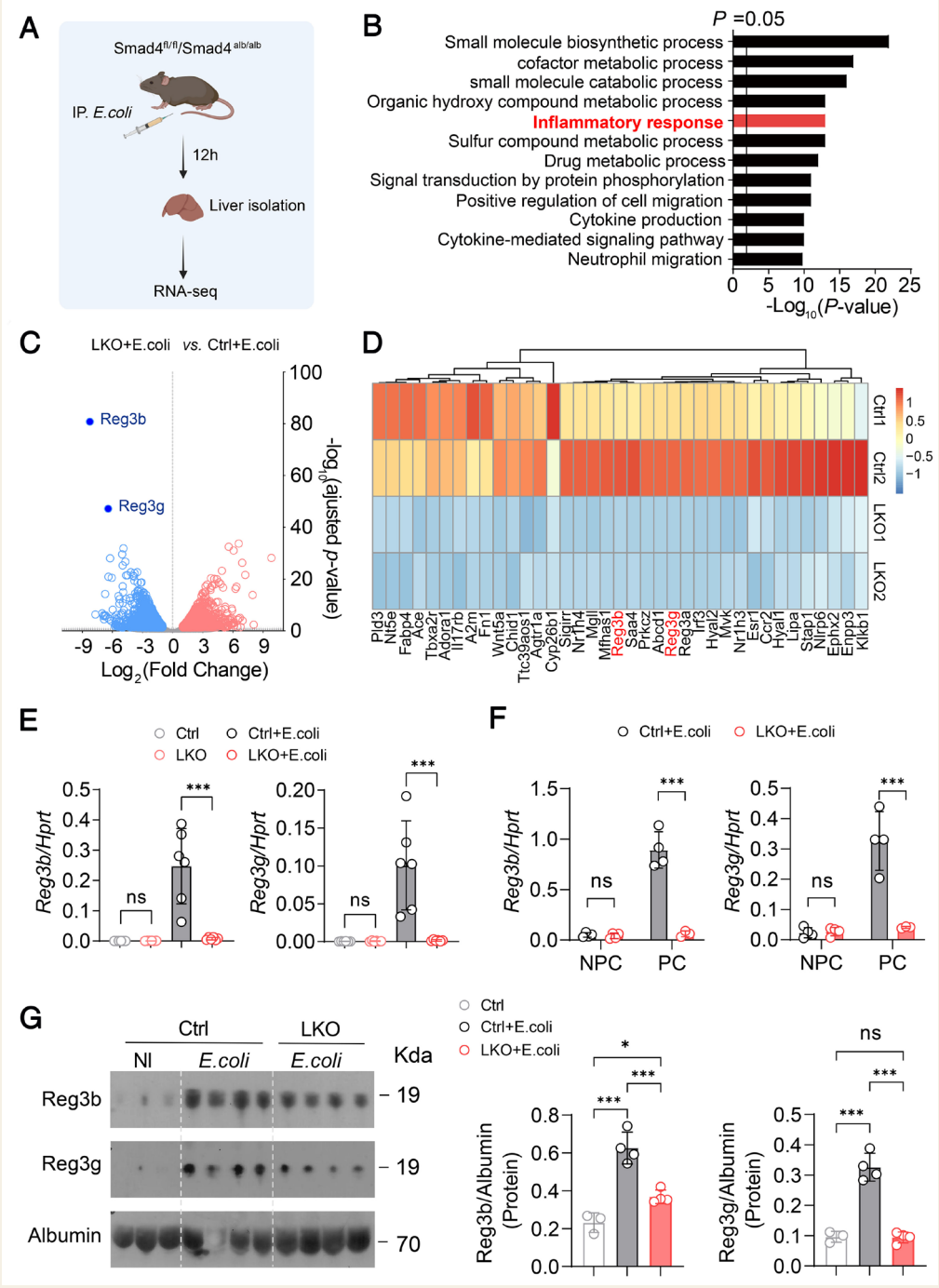

Figure 2. Smad4 deletion in hepatocytes decrease the expression of *Reg3b* and *Reg3g*.
(A) Schematic diagram depicting the strategy for the RNA seq of control and LKO liver 12 h post infection; (B) KEGG Pathway enrichment analysis of genetic programs differentially expressed in the liver from control and LKO mice 12 h post infection; (C) Volcano plot representation of RNA sequencing data of genes upregulated (red) or downregulated (blue) in the liver from control and LKO mice 12 h post infection. Gray dots indicate genes that were not significantly upregulated or downregulated; (D) Heat map representation of inflammatory response-related genes differentially expressed in the liver of control and LKO mice 12 h post infection; (E) Quantitative PCR of *Reg3b* and *Reg3g* in the liver samples taken from control and LKO mice (non-infected and 12 h post *E. coli* infection, respectively) ($n = 6$ per group); (F) The mRNA level of *Reg3b* and *Reg3g* in the parenchymal cell and non-parenchymal cell of control ($n = 4$) and LKO mice ($n = 4$) 12 h postinfection; (G) The protein levels and respective quantification of *Reg3b* and *Reg3g* in the serum of untreated ($n = 3$), control + *E. coli* ($n = 4$) and LKO + *E. coli* mice ($n = 4$). Circles correspond to individual mouse. Results are represented as mean ± SD and are obtained at 6 weeks of age. The membrane only detects a single protein and the area outside the target band is blank or has no effective signal. The *P* values in (E and F) were determined using unpaired Student's *t*-tests. The *P* values in (G) were determined using one-way ANOVA. $^{*}P < 0.05$; $^{***}P < 0.001$. NS: Not significant; IP: intraperitoneal injection; *E. coli*: *Escherichia coli*; NI: non-infected; KEGG: Kyoto Encyclopedia of Genes and Genomes; LKO: liver-specific Smad4 knockout.

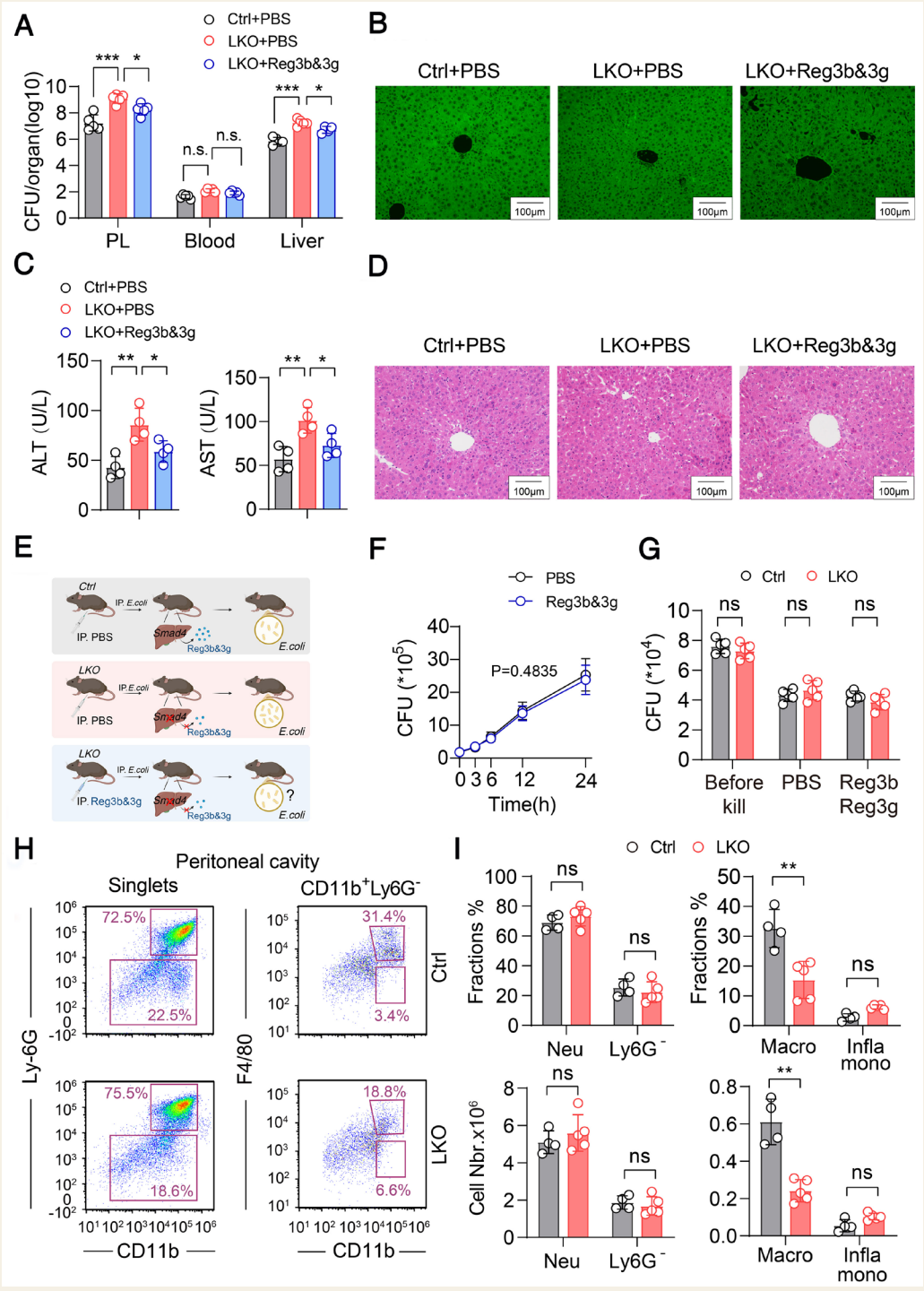

Figure 3. The supplementation of *Reg3b* and *Reg3g* exert protective effects on LKO mice during infection.
(A) The LKO mice were injected intraperitoneally with 1ug of mouse recombinant *Reg3b* and *Reg3g* (rReg3b and rReg3g) or PBS at the time of *E. coli* infection. The mice were sacrificed 12 h post infection and analysis for bacterial CFU counts in the peritoneal fluid, blood and liver ($n = 5$ per group); (B) Fluorescence microscopy of liver tissues of control, LKO + PBS, LKO + r*Reg3b* and *Reg3g* mice infected with GFP-labeled *E. coli*; (C) Serum ALT and AST levels of control, LKO + PBS, LKO + rReg3b and rReg3g mice were measured 12 h post infection ($n = 4$ per group); (D) Representative hematoxylin and eosin staining of liver tissue in control, LKO + PBS and LKO + rReg3b and rReg3g mice 12 h post infection; (E) Schematic diagram illustrating the experimental design and potential anti-bacteria mechanism of rReg3b and rReg3g treatment for LKO mice; (F) The CFU counts of *E. coli* after exposure to recombinant *Reg3b* and *Reg3g in vitro* ($n = 3$ per group); (G) Bacterial killing capacity of control, LKO macrophages and LKO macrophages treated with rReg3b and rReg3g, following stimulation with *E. coli* ($n = 5$ per group); (H) Representative flow cytometry dot plot of macrophages, monocytes and myeloid cells in the peritoneal fluid of control ($n = 4$) and LKO mice ($n = 5$); (I) Representative cell proportion and number of macrophages, monocytes and myeloid cells in

the peritoneal fluid of control (n = 4) and LKO mice (n = 5). Circles correspond to individual mouse. Results are represented as mean ± SD. The P values in (A, C) were determined using one-way ANOVA. The P values in (F) were determined using unpaired Student's t-tests. The P values in (G, I) were determined using two-way ANOVA. *P < 0.05; **P < 0.01; ***P < 0.001. NS: Not significant; CFU: colony forming unit; PBS: phosphate buffered saline; LKO: liver-specific Smad4 knockout; GFP: green fluorescent protein; *E. coli*: *Escherichia coli*; ALT: alanine transaminase; AST: aspartate transaminase.

We further validated the results using qRT-PCR on liver samples collected 12 h post infection. Consistent with our RNA-seq results, we found that the elevated transcription of *Reg3b* and *Reg3g* induced by *E. coli* infection was abolished in the Smad4-deficient liver [Figure 2E], reinforcing the idea that *Reg3b* and *Reg3g* might be the downstream genes of Smad4. To determine which compartment in the liver was responsible for *Reg3b* and *Reg3g* expression, we isolated hepatocytes (hepatic parenchymal cells, PC) and hepatic non-parenchymal cells (NPC) using perfusion plus enzyme digestion from *E. coli* infected LKO or control mice. The results revealed that *Reg3b* and *Reg3g* were mainly expressed in hepatocytes (PC) but not in NPC [Figure 2F]. Additionally, we also evaluated the expression of *Reg3b*/*Reg3g* in extrahepatic organs (intestine, kidneys, heart and spleen) before and after bacterial infection. The result revealed that the expression levels of *Reg3b*/*Reg3g* showed no significant difference in the kidney, heart, and spleen pre and post infection [Extended Support Figure 2E-G], whereas their expression in the intestine was slightly higher after infection in control mice [Extended Support Figure 2H]. Meanwhile, we also noticed that their expression did not differ between control and Smad4 KO mice after infection. Given that Reg3 family function as secretory proteins[29,30], we asked whether the reduction of *Reg3b* and *Reg3g* mRNA expression would affect the circulating level. Indeed, the serum levels of *Reg3b* and *Reg3g* proved markedly decreased in the infected LKO mice *vs.* Ctrl mice [Figure 2G]. These results suggest that Smad4 in hepatocytes supports the expression of *Reg3b* and *Reg3g* in the liver and their subsequent secretion into the circulation upon bacterial infection.

Supplementation of recombinant *Reg3b* and *Reg3g* protected LKO mice from bacterial infection

As Reg3 family has been reported to participate in inflammatory response[31,32], we sought to explore whether the increased susceptibility to bacterial infection of LKO mice was attributed to decreased *Reg3b* and *Reg3g* expression. To test this, we administered recombinant *Reg3b* and *Reg3g* protein to infected LKO mice right after the *E. coli* inoculation. Notably, 12 h after infection, the supplementation of REG3B and REG3G significantly reduced the bacteria loading in the peritoneal fluid and liver of infected LKO mice in comparison to the control group, while there was no difference in the blood [Figure 3A and B]. Additionally, this treatment potently mitigated the liver injury of infected LKO mice, as assessed by serum ALT and AST levels [Figure 3C], along with HE staining [Figure 3D]. Collectively, these data suggested that *Reg3b* and *Reg3g* serve as the key factors for the anti-bacterial activity in mice and that their deficiency contributes to the infection susceptibility observed in Smad4-deficient mice.

Reg3b and *Reg3g* exert anti-bacterial activity through recruitment of macrophages

We next aim to investigate how *Reg3b*/Reg3g exert their anti-bacterial function [Figure 3E]. Given that *Reg3b* and *Reg3g* are reported as antibacterial peptides and may have antimicrobial activity against bacterial[33,34]; We firstly tested this hypothesis by directly incubating recombinant *Reg3b* and *Reg3g* with *E. coli*. However, the number of colony forming units (CFUs) was not reduced upon exposure to *Reg3b* and *Reg3g*, indicating no direct bactericidal effect against this pathogen [Figure 3F]. Since macrophages serve as the main effector cells for clearing bacteria in sepsis, and Reg3 family protein may act on macrophage[35], we next investigated whether *Reg3b/3g* regulates the inherent antibacterial activities or the migration of macrophages. Pre-incubation with recombinant *Reg3b* and *Reg3g* did not enhance the intrinsic bactericidal capacity of macrophages against *E. coli* [Figure 3G], suggesting that their function is not mediated by boosting macrophage killing. Further, we performed flow cytometry (FACs) analysis to assess the effect of decreased *Reg3b/3g* on the composition of neutrophils (Ly-6G$^+$CD11b$^+$), monocytes (F4/80-CD11b$^+$) and macrophages (F4/80$^+$CD11b$^+$) in the infected mice. Interestingly, we found the proportion and number of macrophages decreased significantly in the peritoneal cavity of LKO mice, while the proportion and number of neutrophils were not significantly changed [Figure 3H and I]. As the migration of macrophages could also be mediated by a series of chemokines, we measured the expression level of several macrophage chemotaxis-related genes (*CCl2, CCl3, CCl4, CCl5, CCl7, CCl8, Cxcl10,* and *Cx3cl1*) in the liver of LKO mice [Extended Support Figure 3A]. The result indicated that the transcript levels for these genes appeared either comparable or increased than those in control mice, which may not account for the reduced macrophage in LKO mice. Additionally, under uninfected conditions, the percentage and count of macrophages in the peritoneal cavity and liver of LKO mice were similar to those observed in control mice [Extended Support Figure 3B and C]. Collectively, these findings suggested that the *Reg3b* and *Reg3g* production in the liver facilitates the recruitment of macrophages and monocytes upon bacterial infection.

In addition, to examine whether the higher mortality of LKO mice upon bacterial infection is associated with impaired macrophage recruitment, we utilized the giant cell scavenger CL (disodium clodronate liposome)[36] to deplete the phagocytes (including macrophages) of mice [Extended Support Figure 4A]. Notably, the difference of susceptibility to *E. coli* between LKO and control mice was abolished by phagocytes depletion via CL [Figure 4A]. Moreover, the bacterial load and liver injury index were also comparable of the two groups [Figure 4B and C]. Together, these results suggested that the reduced macrophage recruitment might lead to the vulnerability in LKO mice against bacterial infection.

Then, we conducted flow cytometry assay to investigate whether this supplementation with *Reg3b* and *Reg3g* could rescue the impaired cell migration of LKO mice. In the peritoneal cavity, the treatment of *Reg3b* and *Reg3g* effectively restored the number of macrophages compared to vehicle-treated LKO mice [Figure 4D and E], whereas the proportion and number of inflammatory monocytes in the blood was not significantly changed [Extended Support Figure 4B]. Additionally, we performed flow cytometry experiments to assess the polarization of macrophage. The result revealed that there was no preferential defect regarding polarization in the peritoneal cavity of LKO mice, as both M1 and M2-like macrophages were equally reduced, while supplementation of *Reg3b*/*Reg3g* restored this defect [Extended Support Figure 4C and D]. In the liver, we observed an increased trend of M1-like macrophage in LKO while no difference in M2-like macrophage when compared to control mice [Extended Support Figure 4E and F]. Furthermore, we treated

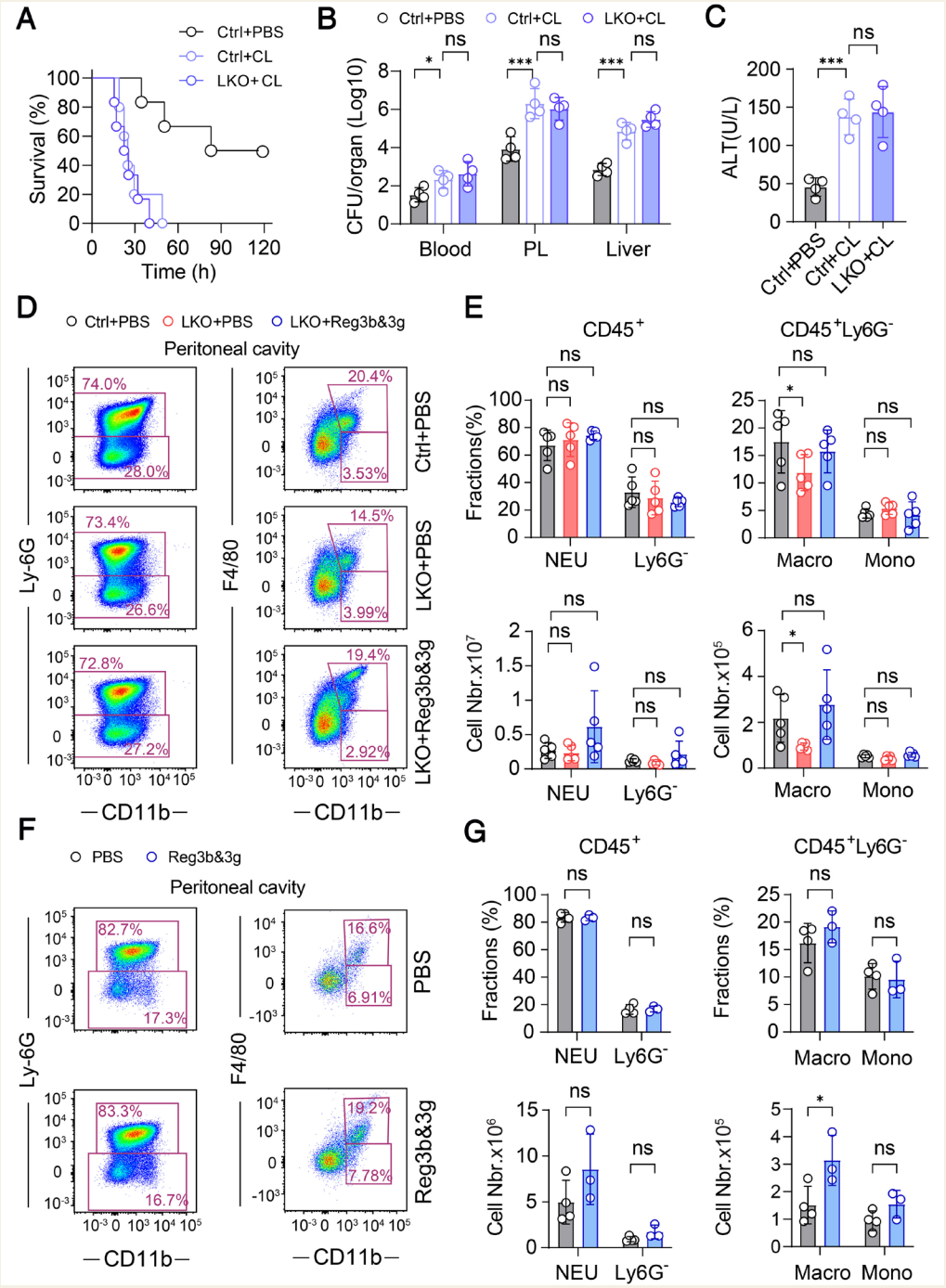

Figure 4. *Reg3b* and *Reg3g* exert anti-bacterial activity through recruiting macrophages.
(A) The Kaplan-Meier survival curve of control mice ($n = 6$) , LKO mice treated with PBS (LKO + PBS) ($n = 5$) and LKO mice treated with clodronate liposomes (LKO + CL) ($n = 6$) upon *E. coli* infection; (B) Bacterial CFU counts were measured in the peritoneal fluid, blood and liver of control ($n = 4$), LKO + PBS ($n = 4$) and LKO + CL mice ($n = 4$) 12 h post *E. coli* infection; (C) The level of ALT and AST in the serum of control ($n = 4$), LKO + PBS ($n = 4$) and LKO + CL mice ($n = 4$) 12 h post infection; (D) Representative flow cytometry dot plot of neutrophils, macrophages and monocytes in the peritoneal fluid of control, LKO + PBS and LKO + rReg3b and rReg3g mice; (E) The corresponding proportion and cell number of neutrophils, macrophages and monocytes in the peritoneal fluid of control ($n = 5$), LKO + PBS ($n = 5$) and LKO + rReg3b and rReg3g mice ($n = 5$); (F) Representative flow cytometry dot plot of neutrophils, macrophages and monocytes in the peritoneal fluid of WT + PBS ($n = 4$) and WT + rReg3b and rReg3g mice ($n = 3$); (G) The corresponding proportion and cell number of neutrophils, macrophages and monocytes in the peritoneal fluid of WT + PBS ($n = 4$) and WT + rReg3b and rReg3g mice ($n = 3$). Circles correspond to individual mouse. Results are represented as mean ± SD. *P* values in (A) were determined using log-rank (Mantel-Cox) test. The *P* values in (C) were determined using one-way ANOVA. The *P* values in (B, E and G) were determined using two-way ANOVA. $^{*}P < 0.05$; $^{***}P < 0.001$. NS: Not significant; *E. coli*: *Escherichia coli*; ALT: alanine transaminase; AST: aspartate transaminase; CFU: colony forming unit; WT: wild type; LKO: liver-specific Smad4 knockout; PBS: phosphate buffered saline.

the wildtype mice with *Reg3b* and *Reg3g*, and found the count of macrophages as well as inflammatory monocytes within the peritoneal cavity and bloodstream showed a rising trend compared to that in vehicle-treated animals [Figure 4F and G, Extended Support Figure 4G and H], while no significant changes were observed in the liver [Extended Support Figure 5A]. In line with these observations, the bacterial load was lower in *Reg3b/3g* treated mice [Extended Support Figure 5B]. These data indicated that supplementation of *Reg3b* and *Reg3g* promotes the recruitment of macrophages, rescue the defect in LKO mice, and also exert a protective effect in wildtype mice upon bacterial infection.

Glucocorticoids and IL-6 act as the upstream stimuli to induce the expression of *Reg3b* and *Reg3g*

To further elucidate the molecular mechanism by which Smad4 regulates *Reg3b* and *Reg3g*, we treated the primary hepatocytes with various stimuli. As Smad4 acts as the central mediator of the TGF-β signaling, we first asked whether TGF-β family ligands induce *Reg3b/3g* expression. However, the treatment of several ligands, including Activin a, Bmp4 and TGF-β, on the primary hepatocytes failed to induce the expression of *Reg3b/3g* [Figure 5A]. Additionally, the exposure of hepatocytes to LPS or heat-inactivated *E. coli* (HK) failed to increase the expression levels of these two genes either [Extended Support Figure 5C]. Notably, previous studies have reported glucocorticoids (GC) and IL-6 could activate the transcription of *Reg3b* in pancreatic cells[37]. In the current study, we utilized glucocorticoids, such as dexamethasone (Dex) and hydrocortisone (Hyd), in combination with IL-6, to examine their potential to induce the upregulation of *Reg3b* and *Reg3g* in primary hepatocytes. The result revealed that while GCs plus IL-6 significantly induced *Reg3b* and *Reg3g* expression, this induction was completely abrogated in Smad4-deficient hepatocytes [Figure 5B]. These findings imply that the GC/IL-6 co-activation of *Reg3b* and *Reg3g* transcription is dependent on the functional integrity of the Smad4 signaling pathway.

We next employed a specific glucocorticoid receptor (GR) inhibitor RU486 to investigate the role of GR signaling in the regulation of *Reg3b* and *Reg3g*[38]. The result of RNA-seq analysis revealed that upon *E. coli* challenge, the transcript levels for *Reg3b* as well as *Reg3g* within the liver were dramatically upregulated 12 h post infection [Figure 5C], similar to Extended Support Figure 2C. However, the increased effect was inhibited after the treatment of RU486, and *Reg3b* and *Reg3g* were among the most downregulated genes in the volcano plot when compared to vehicle-treated controls [Figure 5D]. The qRT-PCR analysis further confirmed suppression of *Reg3b* and *Reg3g* expression following GR inhibition [Figure 5E]. Moreover, the flow cytometry assay revealed that RU486 treatment markedly decreased the count of macrophages and inflammatory monocytes in the liver [Figure 5F and G], and failed to affect monocyte proportions within blood [Figure 5H and I]. Accordingly, we also observed higher bacterial burden [Figure 5J] and greater liver injury index [Figure 5K] in RU486-treated mice than controls, underscoring the essential role of GR signaling in regulating *Reg3b/3g* expression and antibacterial defense.

Since signal transducer and activator of transcription 3 (STAT3) act as the primary downstream transcription factor of IL-6, we thus asked whether Stat3 signaling is required for hepatic Reg3 expression using hepatocyte-specific Stat3 knockout mice (Stat3 LKO). Notably, the result of RNA-seq analysis identified acute-phase response as the significant affected pathways within the liver of *E. coli*-challenged Stat3 LKO mice compared to *E. coli* challenged control [Extended Support Figure 5D]. The result of qRT-PCR also confirmed that the abrogation of *Reg3b* and *Reg3g* expression in infected Stat3 LKO livers [Extended Support Figure 5E]. Moreover, the Stat3 LKO mice exhibited markedly higher mortality [Extended Support Figure 5F] and exacerbated liver injury [Extended Support Figure 5G] following bacterial challenge. Collectively, these data demonstrate that Smad4 is essential for GR/IL-6-induced *Reg3b* and *Reg3g* expression, and identify both GR and STAT3 as crucial transcriptional regulators of these genes during bacterial infection.

Smad4 regulates the transcriptional activity of *Reg3b* and *Reg3g* via Stat3 and GR

We next sought to explore how Smad4 acts on the Stat3-GR mediated *Reg3b*/*Reg3g* expression. Firstly, we assessed whether Smad4 influences the protein levels of STAT3 or GR in the liver of control and LKO mice post infection [Extended Support Figure 6A and B]. Immunoblot analysis indicated that the expression levels of STAT3 or GR showed no substantial change in LKO liver compared to control, suggesting that Smad4 does not regulate *Reg3b* and *Reg3g* by altering the abundance of these transcription factors.

Based on reports that GR and Stat3 could interact with Smad signaling through protein-protein interaction[39,40], we proposed that Smad4 might be involved in the downstream of STAT3 and GR pathway to regulate *Reg3b* and *Reg3g* transcription. To verify this, we performed chromatin immunoprecipitation (ChIP) assays using anti-Smad4 antibody on liver tissues from uninfected control, *E. coli*-infected control and LKO mice. Analysis of Smad4-binding elements (SBEs) in the *Reg3b* and *Reg3g* promoters revealed no enhanced binding of Smad4 upon infection in control mice, and a mild reduction of binding in infected KO mice *vs.* infected control mice [Figure 6A and B]. Of note, the binding of Smad4 to SBEs in all groups was similar to immunoglobulin G (IgG), suggesting a weak direct binding of Smad4 on the promoters of *Reg3b* and *Reg3g*.

We then examined whether Smad4 affects the binding of phosphorylated STAT3 (p-STAT3) to these promoters. Notably, the result showed that the binding capacity of p-Stat3 to *Reg3b*/*Reg3g* promoter showed marked elevation in the liver of control mice infected by *E. coli*, while this was abolished in LKO liver [Figure 6C and D]. Additionally, GR binding to the *Reg3b* and *Reg3g* promoters was enhanced following infection in the liver of control mice, but this enhancement was lost in LKO livers [Extended Support Figure 6C and D]. Collectively, these findings indicate that Smad4 is essential for this binding of both p-STAT3 and GR to the *Reg3b* and *Reg3g* promoters during infection, but does not directly bind these promoters itself. Thus, Smad4 likely acts as an essential co-factor that modulates the transcriptional activity of the *Reg3b* and *Reg3g*. These findings reveal a sophisticated cooperative mechanism wherein Smad4 integrates STAT3 and GR signaling to finely regulate *Reg3b* and *Reg3g* expression during bacterial infection.

DISCUSSION

The present study demonstrated that hepatic Smad4 are responsible for the expression of the acute phase proteins-*Reg3b* and *Reg3g* and protect mice from lethal bacterial infection. In the infection model by *Escherichia coli*, the LKO mice exhibit more bacterial loading and less macrophages or inflammatory monocytes infiltration in the peritoneal cavity. This heightened sensitivity can be mitigated by the addition of recombinant *Reg3b* and *Reg3g* proteins. Moreover, our studies have established that the Smad4-*Reg3b/3g* axis in the liver was modulated by the synergistic effects of GR and Stat3, and is independent of canonical TGF-β signaling pathway.

The TGF-β/Smad signaling cascade exerts a complex and multifaceted function within the pathophysiology in sepsis. TGF-β possesses both anti-inflammatory and pro- inflammatory properties, which

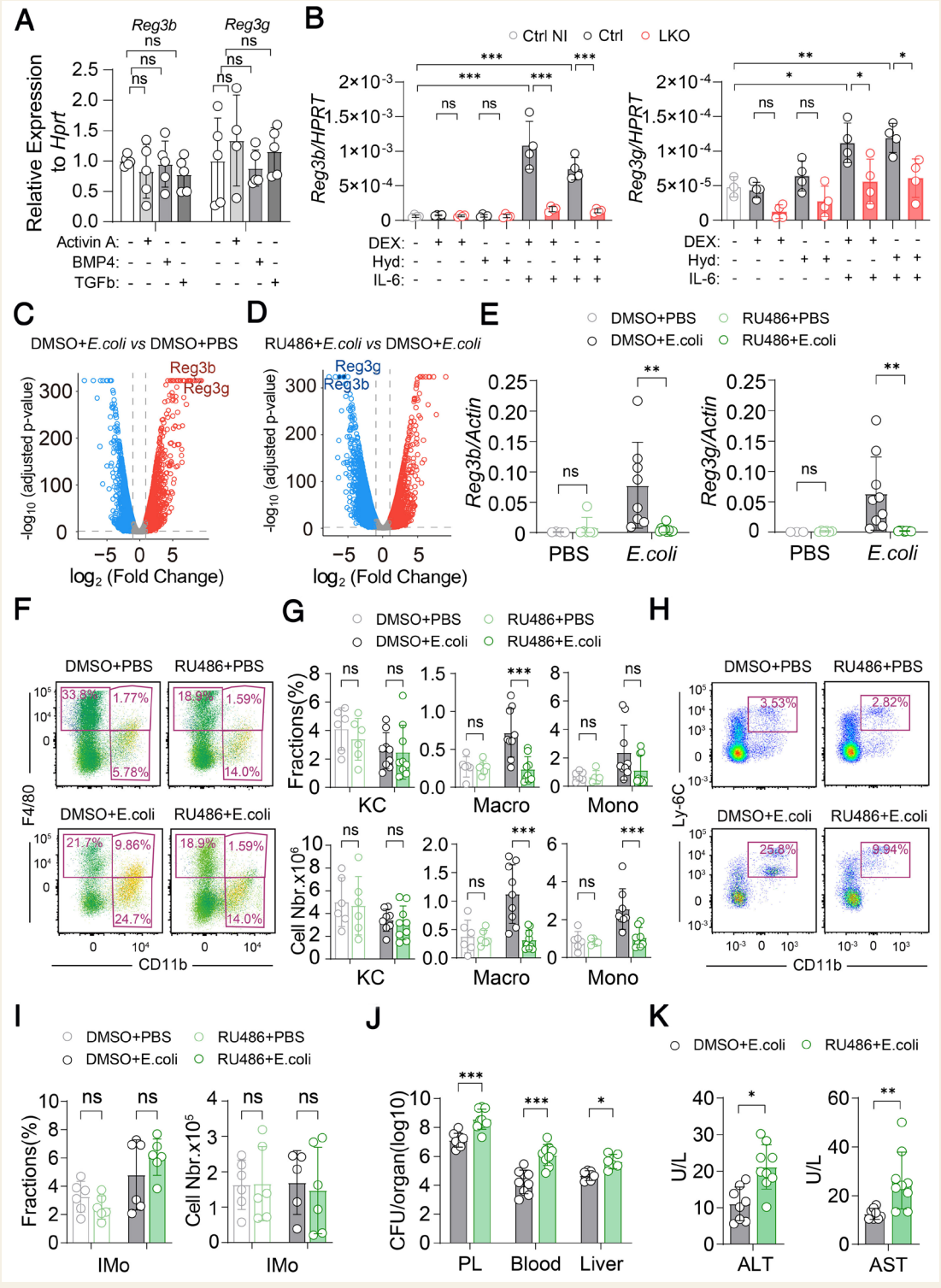

Figure 5. Glucocorticoids/IL-6 acts as the co-activator of *Reg3b* and *Reg3g* transcription.
(A) The mRNA levels of *Reg3b* and *Reg3g* measured in primary hepatocytes isolated from WT mice and treated with TGF-β, Activin a, or BMP4 for 12 h (n = 5 per group); (B) The mRNA level of *Reg3b* and *Reg3g* measured in primary hepatocytes isolated from control and LKO mice and differentially treated with Dex, Hyd, IL6 (n = 4 per group); (C) Volcano plot representation of RNA sequencing data of genes upregulated (red) or downregulated (blue) in the liver from WT mice (non-infected) and WT mice infected with *E. coli* (12 h postinfection). Gray dots indicate genes that were not significantly upregulated or downregulated; (D) Volcano plot representation of RNA sequencing data of genes upregulated (red) or downregulated (blue) in the liver from *E. coli* infected WT mice and WT + RU486 mice (12 h post infection). Gray dots indicate genes that were not significantly upregulated or downregulated; (E) The mRNA level of *Reg3b* and *Reg3g* in

the liver of WT mice and WT + RU486 mice (at non-infected conditions and upon *E. coli* infection) (n = 6-9 per group); (F) Representative flow cytometry dot plot of Kupffer cells, macrophage and Monocytes in the liver of WT mice and WT + RU486 mice at non-infected conditions and upon *E. coli* infection (n = 6-9 per group); (G) The corresponding cell proportion/number of Kupffer cells, macrophage and Monocytes in the liver of WT mice and WT + RU486 mice at non-infected conditions and upon *E. coli* infection (n = 6-9 per group); (H) Representative flow cytometry dot plot of inflammatory monocytes in the blood of WT mice and WT + RU486 mice (at non-infected conditions and upon *E. coli* infection) (n = 6-9 per group); (I) The corresponding cell proportion/number of inflammatory monocytes in the blood of WT mice and WT + RU486 mice (at non-infected conditions and upon *E. coli* infection) (n = 6-9 per group); (J) The bacterial CFU counts in the peritoneal fluid, blood and liver of WT and WT + RU486 mice 12 h post *E. coli* infection (n = 6-9 per group); (K) Serum ALT and AST levels of WT mice and WT + RU486 mice at non-infected conditions and upon *E. coli* infection (n = 6-9 per group). Circles correspond to individual mouse. Results are represented as mean ± SD. The P values in (A) were determined using one-way ANOVA. The P values in (B, E, G, H and I) were determined using two-way ANOVA. The P values in (J) were determined using unpaired Student's t-tests. *P < 0.05; **P < 0.01; ***P < 0.001. NS: Not significant; PBS: phosphate buffered saline; KC: Kupffer cell; DMSO: dimethyl sulfoxide; LKO: liver-specific Smad4 knockout; ALT: alanine transaminase; AST: aspartate transaminase; WT: wild type; TGF-β: transforming growth factor-β; BMP4: bone morphogenetic protein 4; Dex: dexamethasone; Hyd: hydrocortisone; IL-6: interleukin-6; *E. coli*: *Escherichia coli*; RU486: mifepristone; CFU: colony forming unit.

play an essential function in preserving balanced host immunity during inflammatory states. There have been reports that mice over-expressing TGF-β1 in the liver exhibited higher mortality as well as elevated synthesis of inflammatory cytokines (TNF-alpha) in the endotoxin shock model[41]. Notably, TGFβ1 knockout mice together with those deficient in the transcription factor SMAD3 also showed elevated production of inflammatory cytokines as well as nitric oxide, which lead to massive uncontrolled inflammation and endotoxin hyperresponsiveness[42,43]. Despite these paradoxical aspects of TGF-β/Smad pathway in immune regulation, the role of the central factor Smad4 in the host response to infection remained unclear. Here, using the LKO mice model, we demonstrated that these mice were more sensitive to bacterial challenge. According to our results, circulating pro-inflammatory cytokines levels in LKO mice at the early infection stage were only modestly elevated than control, while the bacterial burden was significantly higher, suggesting a defect of bacterial clearance rather than hyperinflammation. Moreover, we observed the number of macrophages derived from LKO mice was significantly reduced upon infection. Taken together, these findings suggest that LKO mice succumb to infection primarily due to immunodeficiency rather than excessive inflammatory response.

The Smad4 LKO mice is characterized by markedly decreased hepcidin expression and consequent iron accumulation in the liver and serum[44]. Notably, the association between iron imbalance and bacterial infection have been reported across several studies[45-49], suggesting that both homeostatic iron regulator (HFE) and hepcidin (products of the *HFE* and *HAMP* genes, respectively) exert protective play protective roles against septic shock[46,47,50]. Using a mouse model of sepsis induced by cecal ligation and puncture, animals that received an adenoviral vector encoding anti-hepcidin short hairpin RNA (shRNA) via intravenous injection exhibited increased death rates along with bacterial load[51]. Interestingly, when we placed LKO mice on an iron-deficient diet to normalize iron levels, the LKO-ID mice remained highly susceptible to *E. coli* infection. Together, these results indicated that aberrant iron accumulation does not significantly contribute to the the increased vulnerability in LKO mice against bacterial challenge.

Beyond its role in hepatocytes, Smad4 functions as a key transducer of TGF-β of TGF-β signaling across diverse immune populations such as B cells, T cells, macrophages and dendritic cells, where it exerts diverse and context-dependent effects on immune homeostasis and pathogen response. In the specific context of liver immunity, a particularly relevant study has demonstrated that the BMP9/BMP10-ALK1-Smad4 signaling axis is essential for maintaining Kupffer cell homeostasis, the liver-resident macrophages. This study showed that ALK1-mediated signaling controls the distinct transcriptional program along with the viability of Kupffer cells via a pathway dependent on Smad4, and that ALK1 deficiency results in defective capture of *Listeria monocytogenes* along with severe systemic infections. Furthermore, Smad4 deficiency in hepatocytes has been shown to attenuate liver inflammation and CXCL1 secretion, indicating that hepatocyte-intrinsic Smad4 signaling also modulates the hepatic inflammatory milieu. Importantly, our present study adds a new dimension to this understanding by demonstrating that Smad4 in hepatocytes regulates the expression of *Reg3b* and *Reg3g* through a non-canonical, TGF-β-independent mechanism involving the synergistic effects of GR and Stat3. Importantly, this Smad4-*Reg3b/3g* axis in hepatocytes does not operate in isolation but rather coordinates with immune cell functions. The *Reg3b/3g* proteins secreted by hepatocytes upon infection act as chemoattractants that recruit macrophages and inflammatory monocytes to the infection site, thereby bridging the innate immune functions of hepatocytes and monocytes/macrophages. The synergistic relationship between hepatocyte Smad4 and immune cell Smad4 in antibacterial immunity can thus be conceptualized as follows: Smad4 in immune cells (including Kupffer cells along with macrophages) is intrinsically required for their differentiation, polarization, and functional maturation, while Smad4 in hepatocytes controls the production of *Reg3b/3g* that serve as key signals for immune cell recruitment. Together, these two Smad4-dependent axes - one operating within immune cells to ensure their proper function, and the other operating within hepatocytes to orchestrate immune cell recruitment - cooperate to mount an effective host defense against bacterial infection.

The Reg3 family constitute a group of secreted C-type lectins that has been well established as key players in intestinal mucosal immunity[33]. Under homeostatic conditions, *Reg3b* and *Reg3g* are predominantly expressed in the intestine and pancreas, where they function as secreted antimicrobial peptides that restrict microbial adherence to the gut epithelial lining as well as limit induction of adaptive immunity via commensal bacteria. Specifically, *Reg3g* exerts bactericidal activity against Gram-positive pathogens including *Listeria monocytogenes* and vancomycin- refractory Enterococcus, with its cleaved form mediating bacterial killing by binding to surface-exposed carbohydrate moieties of peptidoglycan[52]. In addition, previous studies have demonstrated that chronic alcohol abuse inhibits intestinal *Reg3b* and *Reg3g* expression, and that deficiency of *Reg3g* and *Reg3b* lead to increased numbers of mucosa-associated bacteria and enhanced bacterial translocation to the mesenteric lymph nodes and liver, thereby accelerating the

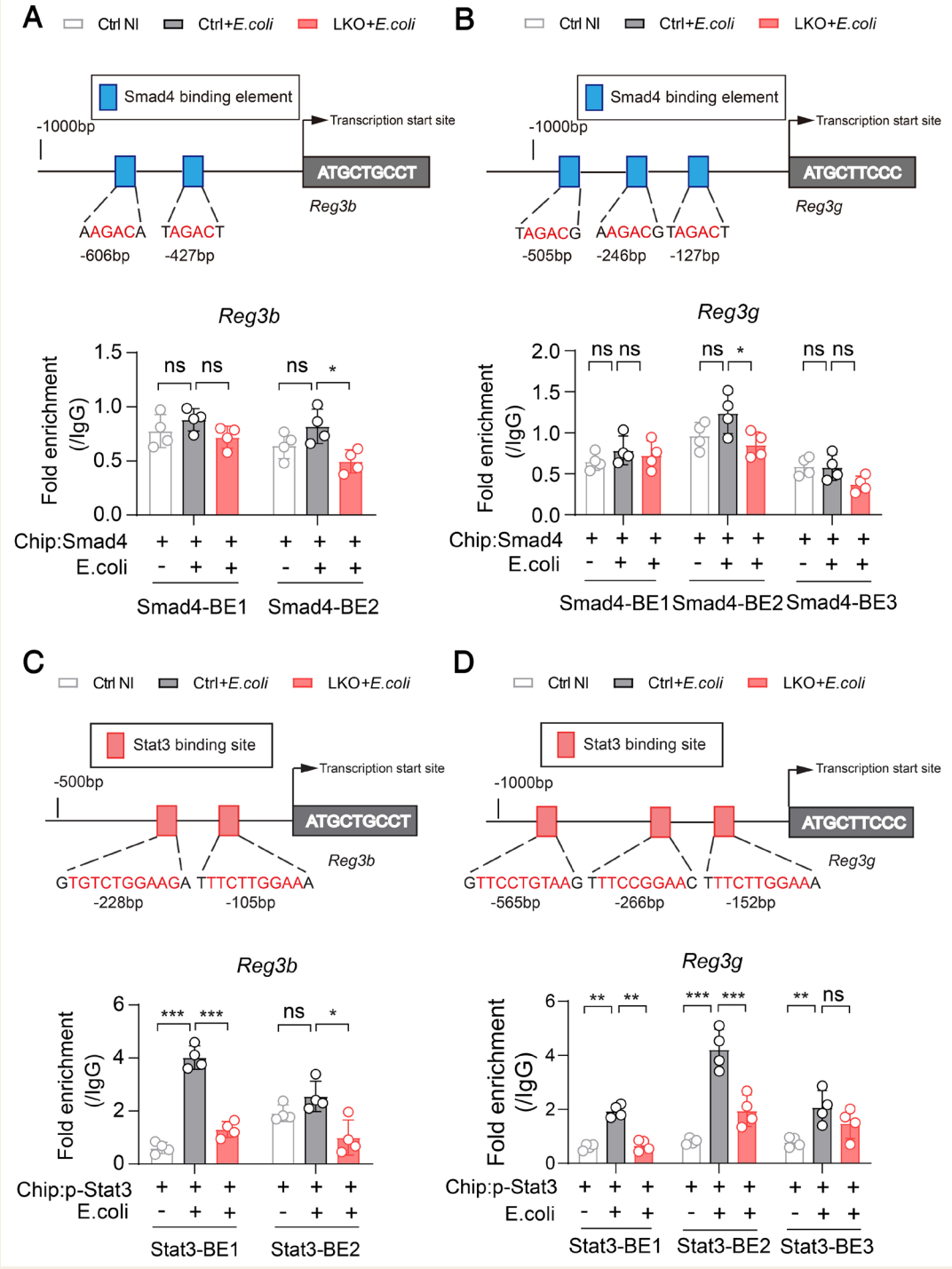

Figure 6. Smad4 regulate the expression of *Reg3b* and *Reg3g* via Stat3 and GR.
(A) ChIP assay using Smad4 antibody followed by qPCR of the *Reg3b* promoter (SMAD4-BE1, SMAD4-BE2) in the liver of non-infected control mice, *E. coli* infected control mice and *E. coli* infected LKO mice (n = 4 per group); (B) ChIP assay using Smad4 antibody followed by qPCR of the *Reg3g* promoter (SMAD4-BE1, SMAD4-BE2 and SMAD4-BE3) in the liver of non-infected control mice, *E. coli* infected control mice and *E. coli* infected LKO mice (n = 4 per group). (C) Stat3 ChIP followed by qPCR of the *Reg3b* promoter (STAT3-BE1 and STAT3-BE2) in the liver of non-infected control mice, *E. coli* infected control mice and *E. coli* infected LKO mice (n = 4 per group); (D) Stat3 ChIP followed by qPCR of the *Reg3g* promoter (STAT3-BE1, STAT3-BE2, STAT3-BE3) in the liver of non-infected control mice, *E. coli* infected control mice and *E. coli* infected LKO mice (n = 4 per group). Circles correspond to individual mouse. Results are represented as mean ± SD. The P values in (A-D) were determined using one-way ANOVA. *P < 0.05; **P < 0.01; ***P < 0.001. NS: Not significant; ChIP: chromatin immunoprecipitation; qPCR: quantitative polymerase chain reaction; *E. coli*: *Escherichia coli*; LKO: liver-specific Smad4 knockout; GR: glucocorticoid receptor.

progression of ethanol-induced fatty liver disease toward steatohepatitis. Conversely, supplementation with prebiotics has been shown to partially restore *Reg3g* protein levels, reduce bacterial overgrowth, and lessen alcoholic steatohepatitis[53,54]. Importantly, however, the present study reveals a previously underappreciated function of *Reg3b* and *Reg3g* in the liver during systemic infection. While intestinal Reg3 proteins primarily act locally to maintain barrier integrity and prevent bacterial translocation from the gut lumen, our findings demonstrate that hepatic expression of *Reg3b* and *Reg3g* is markedly up-regulated upon infection and plays a critical role in bacterial clearance at the systemic level. The antimicrobial effects of Reg3 protein have been reported in several aspects. Specifically, *Reg3g* has bactericidal activity against Gram-positive bacteria[33], as well as a regulatory effect on macrophage differentiation[55]. In the case of *Reg3b*, it has been shown that intestinal secreted *Reg3b* protects mice against infection and dissemination of *Salmonella enteritidis*, a Gram-negative bacterium[56]. Notably, our *in vitro* assays suggest the incubation of *Reg3b/3g* do not exhibit direct bactericidal activity against *E. coli*, nor do they appear to influence the bactericidal capacity of macrophages. Instead, consistent with prior evidence describing *Reg3b* and *Reg3g* as chemoattractants for macrophage migration[57,58], we found that the treatment of recombinant *Reg3b* and *Reg3g* potently restored the decreased macrophage number observed in LKO mice. Thus, the hepatic *Reg3b* and *Reg3g* contribute to the defense against bacterial infections by facilitating macrophage recruitment and proinflammatory monocytes toward the location of infection, a mechanism distinct from the direct antimicrobial function of intestinal Reg3 proteins.

Given that *Reg3b* and *Reg3g* have been reported to be regulated by Il-6/Stat3 pathway[59,60], it is particularly noteworthy that our work linked Smad4 as another novel essential regulator. Importantly, our observations suggested that the expression of *Reg3b* and *Reg3g* does not rely on canonical TGF-β signaling, as neither TGF-β nor Activin A fail to stimulate their expression in primary hepatocytes. Instead, the combination of IL-6 and dexamethasone exerts an activation effect, and this synergistic effect was abolished in the absence of Smad4. Previous reports indicated that IL-6-activated STAT3 associated with GR to form a transcriptional complex, which regulate signal transduction through either IL-6-responsive element (IL-6 RE) or glucocorticoid-responsive element (GRE)[61]. In our study, it seemed that Smad4 does not directly associate with the promoter of *Reg3b* and *Reg3g*. Interestingly, we found the binding capacity of p-Stat3 and GR with the promoter region of *Reg3b* and *Reg3g* was enhanced upon infection, and this enhancement was dampened in the context of Smad4 deficiency. Based on our results, we speculate that Smad4 might be involved in STAT3 and GR signaling and act as a critical co-activator, thereby regulating the transcription expression of *Reg3b* and *Reg3g*.

Limitations of the study

Despite the novel insights provided by this work, several limitations should be acknowledged. Firstly, the infection model employed in this study primarily utilized intraperitoneal injection of *Escherichia coli*; whether the Smad4-*Reg3b/3g* axis operates similarly in other clinically relevant infection routes (e.g., intravenous or intrapulmonary) or against other Gram-negative or Gram-positive pathogens remains to be determined. Secondly, although the iron-deficient diet experiments suggested that iron overload does not primarily account for the susceptibility phenotype, we cannot exclude subtle contributions of iron dysregulation in other tissues. Future studies using conditional knockout approaches, alternative infection models, and detailed mechanistic dissection will be necessary to address these limitations and extend our findings.

In summary, we identified a non-canonical aspect of Smad4 in regulating immunologic function in the liver, where it mediates an essential dialogue between hepatocytes and immune cells to orchestrate host defense. This Smad4-*Reg3b/3g* axis is vital for mounting an effective antibacterial response in patients with liver dysfunction, impairment of this signaling pathway might deteriorate the whole situation when encounter infection events. Our findings suggest that discreet therapeutic strategies aimed at modulating Smad4 signaling may help prevent infection-related complications in vulnerable individuals.

DECLARATIONS

Acknowledgments

We thank Dr. Xin-Hua Feng (Life Sciences Institute, Zhejiang University, Hangzhou) for valuable discussions. We also thank the members of the Wang and Min laboratories for helpful discussions. The graphical abstract, figure 2A, and figure 3E were created with BioRender.com.

Authors' contributions

Designed the experiments: Chen, L.; Wu, Q.; Min, J.; Wang, F.
Performed the experiments: Chen, L.; Zhao, W.; Wu, Q.; Min, J.; Wang, F.
Assisted with murine experiments: Chen, L.; Wang, R.; Luo, H. Yu, Y.
Performed the statistical analyses: Chen, L.; Zhao, W.; Lin, C.
Helped with bioinformatics analysis: Song, Z.
Drafted the manuscript: Chen, L.; Zhao, W.; Min, J. Wang, F.
Revised the manuscript: Wang, F.; Min, J.; Chen, L.; Zhao, W.; Wu, Q.; Weiss, G.
Obtained funding and supervised the study: Wang, F; Min, J.
All authors approved the final version of the paper.

Availability of data and materials

All data reported in this study and further information and requests for resources are available from the corresponding authors upon reasonable request.

AI and AI-assisted tools statement

Not applicable.

Financial support and sponsorship

This study was supported by research grants from the National Natural Science Foundation of China (32330047 to Wang, F.; 82471593 to Min, J.; 82030003 and 32171166 to Wu, Q.) and the China Postdoctoral Science Foundation (M642414 to Wu, Q.).

Conflicts of interest

Wang, F. is the Editor-in-Chief of the journal *Element*. Weiss, G. is an Associate Editor for the journal *Element*. Min, J. is a Deputy Editor of the journal *Element*. Wang, F., Weiss, G. and Min, J. were not involved in any stage of the editorial process, including reviewer selection, manuscript handling, or decision-making. The other authors declare that there are no conflicts of interest.

Ethical approval and consent to participate

All animal experiments were performed in compliance with the guide for the care and use of laboratory animals and approved by the Laboratory Animal Welfare and Ethics Review Committee, Zhejiang University (ZJU20250797).

Consent for publication

Not applicable.

GOLD ■ METHODS

Detailed methods are provided in the online version of this paper and include the following:

KEY RESOURCES TABLE
EXPERIMENTAL MODEL AND SUBJECT DETAILS
 o Animal models
METHOD DETAILS
 o PCR genotyping
 o Analyses of serum
 o Liver transcriptomic analysis
 o *In vivo* depletion of macrophage
 o Macrophage-killing assays
 o Collection and culture of peritoneal macrophages (PMs)
 o Chromatin immunoprecipitation (ChIP) assay
 o Measurements of tissue non-heme iron
 o Assessment of bacterial CFU
 o Isolation and culture of primary hepatocytes
 o Real-time PCR
 o Flow cytometric analysis
 o Protein extraction and immunoblotting analysis
QUANTIFICATION AND STATISTICAL ANALYSIS

EXTENDED SUPPORT MATERIALS

CORE ★ AUTHORS

REFERENCES

1. Singer, M. et al. The third international consensus definitions for sepsis and septic shock (Sepsis-3). *JAMA* **315**, 801-10 (2016). https://doi.org/10.1001/jama.2016.0287
2. Giamarellos-Bourboulis, E. J. et al. The pathophysiology of sepsis and precision-medicine-based immunotherapy. *Nat. Immunol.* **25**, 19-28 (2024). https://doi.org/10.1038/s41590-023-01660-5
3. Huang, M.; Cai, S.; Su, J. The pathogenesis of sepsis and potential therapeutic targets. *Int. J. Mol. Sci.* **20**, 5376 (2019). https://doi.org/10.3390/ijms20215376
4. Hotchkiss, R. S.; Karl, I. E. The pathophysiology and tre zatment of sepsis. *N. Engl. J. Med.* **348**, 138-50 (2003). https://doi.org/10.1056/NEJMra021333
5. Jarczak, D.; Kluge, S.; Nierhaus, A. Sepsis - pathophysiology and therapeutic concepts. *Front. Med.* **8**, 628302 (2021). https://doi.org/10.3389/fmed.2021.628302
6. Gola, A. et al. Commensal-driven immune zonation of the liver promotes host defence. *Nature* **589**, 131-6 (2021). https://doi.org/10.1038/s41586-020-2977-2
7. Hammerich, L.; Tacke, F. Hepatic inflammatory responses in liver fibrosis. *Nat. Rev. Gastroenterol. Hepatol.* **20**, 633-46 (2023). https://doi.org/10.1038/s41575-023-00807-x
8. Khakoo, S. I. et al. HLA and NK cell inhibitory receptor genes in resolving hepatitis C virus infection. *Science* **305**, 872-4 (2004). https://doi.org/10.1126/science.1097670
9. Paust, S. et al. Critical role for the chemokine receptor CXCR6 in NK cell-mediated antigen-specific memory of haptens and viruses. *Nat. Immunol.* **11**, 1127-35 (2010). https://doi.org/10.1038/ni.1953
10. Gu, X. et al. New insights into iNKT cells and their roles in liver diseases. *Front. Immunol.* **13**, 1035950 (2022). https://doi.org/10.3389/fimmu.2022.1035950
11. Yao, T.; Maccioni, L.; Guan, Y.; Rodrigues, R. M.; Gao, B. Liver as a key organ for systemic antimicrobial defense. *Hepatol. Commun.* **9**, e0814 (2025). https://doi.org/10.1097/HC9.0000000000000814
12. Li, D.; Wu, M. Pattern recognition receptors in health and diseases. *Sig. Transduct. Target. Ther.* **6**, 291 (2021). https://doi.org/10.1038/s41392-021-00687-0
13. Xu, M. J. et al. Liver is the major source of elevated serum lipocalin-2 levels after bacterial infection or partial hepatectomy: a critical role for IL-6/STAT3. *Hepatology* **61**, 692-702 (2015). https://doi.org/10.1002/hep.27447
14. Medzhitov, R. Recognition of microorganisms and activation of the immune response. *Nature* **449**, 819-26 (2007). https://doi.org/10.1038/nature06246
15. Ehlting, C.; Wolf, S. D.; Bode, J. G. Acute-phase protein synthesis: a key feature of innate immune functions of the liver. *Biol. Chem.* **402**, 1129-45 (2021). https://doi.org/10.1515/hsz-2021-0209
16. Bui, T. M.; Wiesolek, H. L.; Sumagin, R. ICAM-1: a master regulator of cellular responses in inflammation, injury resolution, and tumorigenesis. *J. Leukoc. Biol.* **108**, 787-99 (2020). https://doi.org/10.1002/JLB.2MR0220-549R
17. Gong, J.; Tu, W.; Liu, J.; Tian, D. Hepatocytes: a key role in liver inflammation. *Front. Immunol.* **13**, 1083780 (2023). https://doi.org/10.3389/fimmu.2022.1083780
18. Liu, L. et al. Hepatic IκBζ promotes alcohol-associated liver disease and acute hepatitis by enhancing CXCL1-mediated neutrophil infiltration. *Free Radic. Biol. Med.* **237**, 558-69 (2025). https://doi.org/10.1016/j.freeradbiomed.2025.06.022
19. Lajarin, F.; Rubio, G.; Lorenzo, N.; Gámiz, P.; Hernandez-Caselles, T.; Garcia-Peñarrubia, P. Implication of reactive oxygen species in the antibacterial activity against Salmonella Typhimurium of hepatocyte cell lines. *Free Radic. Biol. Med.* **27**, 1008-18 (1999). https://doi.org/10.1016/s0891-5849(99)00148-3
20. Cui, X.; Song, Y.; Han, J.; Yuan, Z. The multifaceted role of SMAD4 in immune cell function. *Biochem. Biophys. Rep.* **41**, 101902 (2024). https://doi.org/10.1016/j.bbrep.2024.101902
21. Chen, W.; Ten Dijke, P. Immunoregulation by members of the TGFβ superfamily. *Nat. Rev. Immunol.* **16**, 723-40 (2016). https://doi.org/10.1038/nri.2016.112
22. Park, S. R.; Lee, J. H.; Kim, P. H. Smad3 and Smad4 mediate transforming growth factor-β1-induced IgA expression in murine B lymphocytes. *Eur. J. Immunol.* **31**, 1706-15 (2001). https://doi.org/10.1002/1521-4141(200106)31:6<1706::aid-immu1706>3.0.co;2-z
23. Pan, H.; Ding, E.; Hu, M.; Lagoo, A. S.; Datto, M. B.; Lagoo-Deenadayalan, S. A. SMAD4 is required for development of maximal endotoxin tolerance. *J. Immunol.* **184**, 5502-9 (2010). https://doi.org/10.4049/jimmunol.0901601
24. Hahn, J. N.; Falck, V. G.; Jirik, F. R. Smad4 deficiency in T cells leads to the Th17-associated development of premalignant gastroduodenal lesions in mice. *J. Clin. Invest.* **121**, 4030-42 (2011). https://doi.org/10.1172/JCI45114
25. Choi, S. H.; Huang, A. Y.; Letterio, J. J.; Kim, B. G. Smad4-deficient T cells promote colitis-associated colon cancer via an IFN-γ-dependent suppression of 15-hydroxyprostaglandin dehydrogenase. *Front. Immunol.* **13**, 932412 (2022). https://doi.org/10.3389/fimmu.2022.932412
26. Igalouzene, R.; Hernandez-Vargas, H.; Benech, N.; et al. SMAD4 TGF-β-independent function preconditions naive $CD8^+$ T cells to prevent severe chronic intestinal inflammation. *J. Clin. In-*

vest. **132**, e151020 (2022). https://doi.org/10.1172/JCI151020
27. Kowdley, K. V.; Gochanour, E. M.; Sundaram, V.; Shah, R. A.; Handa, P. Hepcidin signaling in health and disease: ironing out the details. *Hepatol Commun.* **5**, 723-35 (2021). https://doi.org/10.1002/hep4.1717
28. Dolmatova, E. V.; Wang, K.; Mandavilli, R.; Griendling, K. K. The effects of sepsis on endothelium and clinical implications. *Cardiovasc. Res.* **117**, 60-73 (2021). https://doi.org/10.1093/cvr/cvaa070
29. Parikh, A.; Stephan, A. F.; Tzanakakis, E. S. Regenerating proteins and their expression, regulation, and signaling. *Bio. Concepts.* **3**, 57-70 (2012). https://doi.org/10.1515/bmc.2011.055
30. Qi, Z. et al. REG/Reg family proteins: mediating gut microbiota homeostasis and implications in digestive diseases. *Gut Microbes* **17**, 2568055 (2025). https://doi.org/10.1080/19490976.2025.2568055
31. Cao, Y.; Tian, Y.; Liu, Y.; Su, Z. Reg3β: a potential therapeutic target for tissue injury and inflammation-associated disorders. *Int. Rev. Immunol.* **41**, 160-70 (2021). https://doi.org/10.1080/08830185.2020.1869731
32. Yao, A.; Huang, C.; Wang, X.; Zhou, R.; Hao, W.; Lin, Q. The Reg protein family: potential new targets for the treatment of inflammatory bowel disease and colorectal cancer. *Front. Gastroenterol.* **3**, 1386069 (2024). https://doi.org/10.3389/fgstr.2024.1386069
33. Cash, H. L.; Whitham, C. V.; Behrendt, C. L.; Hooper, L. V. Symbiotic bacteria direct expression of an intestinal bactericidal lectin. *Science* **313**, 1126-30 (2006). https://doi.org/10.1126/science.1127119
34. Miki, T. et al. RegIIIβ promotes Salmonella Typhimurium colonization of the gut in the early-stage gastrointestinal infection by enhancing flagella-driven locomotion. *PLoS Pathog.* **21**, e1013665 (2025). https://doi.org/10.1371/journal.ppat.1013665
35. Lörchner, H. et al. Reg proteins direct accumulation of functionally distinct macrophage subsets after myocardial infarction. *Cardiovasc. Res.* **114**, 1667-79 (2018). https://doi.org/10.1093/cvr/cvy126
36. Song, Z. et al. Progranulin plays a central role in host defense during sepsis by promoting macrophage recruitment. *Am. J. Respir. Crit. Care Med.* **194**, 1219-32 (2016). https://doi.org/10.1164/rccm.201601-0056OC
37. Luo, C.; Li, B.; Liu, L.; Yin, H. P.; Wang, M.; Liu, J. L. Transcriptional activation of Reg2 and Reg3β genes by glucocorticoids and interleukin-6 in pancreatic acinar and islet cells. *Mol. Cell. Endocrinol.* **365**, 187-96 (2013). https://doi.org/10.1016/j.mce.2012.10.018
38. Lin, C. C.; Cheng, P. Y.; Hsiao, M.; Liu, Y. P. Effects of RU486 in treatment of traumatic stress-induced glucocorticoid dysregulation and fear-related abnormalities: early versus late intervention. *Int. J. Mol. Sci.* **23**, 5494 (2022). https://doi.org/10.3390/ijms23105494
39. Song, C.; Tian, X.; Gelehrter, T. D. Glucocorticoid receptor inhibits transforming growth factor-β signaling by directly targeting the transcriptional activation function of Smad3. *Proc. Natl. Acad. Sci. U S A.* **96**, 11776-81 (1999). https://doi.org/10.1073/pnas.96.21.11776
40. Bryson, B. L.; Junk, D. J.; Cipriano, R.; Jackson, M. W. STAT3-mediated SMAD3 activation underlies oncostatin M-induced senescence. *Cell Cycle* **16**, 319-34 (2017). https://doi.org/10.1080/15384101.2016.1259037
41. Vodovotz, Y. et al. Increased mortality, blunted production of nitric oxide, and increased production of TNF-α in endotoxemic TGF-β1 transgenic mice. *J. Leukocyte Biol.* **63**, 31-9 (1998). https://doi.org/10.1002/jlb.63.1.31
42. Mccartney-Francis, N.; Jin, W.; Wahl, S. M. Aberrant toll receptor expression and endotoxin hypersensitivity in mice lacking a functional TGF-β1 signaling pathway. *J. Immunol.* **172**, 3814-21 (2004). https://doi.org/10.4049/jimmunol.172.6.3814
43. Lv, K. Y. et al. Deficiency of Smad3 results in enhanced inducible nitric oxide synthase-mediated hypotension in lipopolysaccharide-induced endotoxemia. *J. Surg. Res.* **187**, 640-5 (2014). https://doi.org/10.1016/j.jss.2013.11.1090
44. Wang, R. H. et al. A role of SMAD4 in iron metabolism through the positive regulation of hepcidin expression. *Cell Metab.* **2**, 399-409 (2005). https://doi.org/10.1016/j.cmet.2005.10.01
45. Schaible, U. E.; Collins, H. L.; Priem, F.; Kaufmann, S. H. Correction of the iron overload defect in β-2-microglobulin knockout mice by lactoferrin abolishes their increased susceptibility to tuberculosis. *J. Exp. Med.* **196**, 1507-13 (2002). https://doi.org/10.1084/jem.20020897
46. Gomes-Pereira, S.; Rodrigues, P. N.; Appelberg, R.; Gomes, M. S. Increased susceptibility to mycobacterium avium in hemochromatosis protein HFE-deficient mice. *Infect. Immun.* **76**, 4713-9 (2008). https://doi.org/10.1128/IAI.00612-08
47. Arezes, J. et al. Hepcidin-induced hypoferremia is a critical host defense mechanism against the siderophilic bacterium Vibrio vulnificus. *Cell Host Microbe* **17**, 47-57 (2015). https://doi.org/10.1016/j.chom.2014.12.001
48. Mu, Q. et al. The role of iron homeostasis in remodeling immune function and regulating inflammatory disease. *Sci. Bull.* **66**, 1806-16 (2021). https://doi.org/10.1016/j.scib.2021.02.010
49. Wu, Q. et al. Hemojuvelin regulates the innate immune response to peritoneal bacterial infection in mice. *Cell Discov.* **3**, 17028 (2017). https://doi.org/10.1038/celldisc.2017.28
50. De Domenico, I. et al. Hepcidin mediates transcriptional changes that modulate acute cytokine-induced inflammatory responses in mice. *J. Clin. Investig.* **120**, 2395-405 (2010). https://doi.org/10.1172/JCI42011
51. Zeng, C.; Chen, Q.; Zhang, K.; Chen, Q.; Song, S.; Fang, X. Hepatic hepcidin protects against polymicrobial sepsis in mice by regulating host iron status. *Anesthesiology* **122**, 374-86 (2015). https://doi.org/10.1097/ALN.0000000000000466
52. Brandl, K.; Plitas, G.; Schnabl, B.; Dematteo, R. P.; Pamer, E. G. MyD88-mediated signals induce the bactericidal lectin RegIIIγ and protect mice against intestinal Listeria monocytogenes infection. *J. Exp. Med.* **204**, 1891-900 (2007). https://doi.org/10.1084/jem.20070563
53. Yan, A. W. et al. Enteric dysbiosis associated with a mouse model of alcoholic liver disease. *Hepatology* **53**, 96-105 (2011). https://doi.org/10.1002/hep.24018
54. Wang, L. et al. Intestinal REG3 lectins protect against alcoholic steatohepatitis by reducing mucosa-associated microbiota and preventing bacterial translocation. *Cell Host Microbe* **19**, 227-39 (2016). https://doi.org/10.1016/j.chom.2016.01.003
55. Gironella, M. et al. Reg3β deficiency impairs pancreatic tumor growth by skewing macrophage polarization. *Cancer Res.* **73**, 5682-94 (2013). https://doi.org/10.1158/0008-5472.CAN-12-3057

56. van Ampting, M. T. J. et al. Intestinally secreted C-Type lectin Reg3b attenuates salmonellosis but not listeriosis in mice. I*nfect. Immun.* **80**, 1115-20 (2012). https://doi.org/10.1128/IAI.06165-11
57. Namikawa, K.; Okamoto, T.; Suzuki, A.; Konishi, H.; Kiyama, H. Pancreatitis-Associated Protein-III Is a novel macrophage chemoattractant implicated in nerve regeneration. *J. Neurosci.* **26**, 7460-7 (2006). https://doi.org/10.1523/JNEUROSCI.0023-06.2006
58. Lörchner, H. et al. Myocardial healing requires Reg3β-dependent accumulation of macrophages in the ischemic heart. *Nat. Med.* **21**, 353-62 (2015). https://doi.org/10.1038/nm.3816
59. Cineus, R. et al.; TRR241 IBDome Consortium. The IL-22-oncostatin M axis promotes intestinal inflammation and tumorigenesis. *Nat. Immunol.* **26**, 837-53 (2025). https://doi.org/10.1038/s41590-025-02149-z
60. Yang, Z. et al. BAF60C links nucleolar stress to β cell dysfunction in type 2 diabetes through controlling Reg3b mRNA decay. *Dev. Cell* **61**, 976-94.e11 (2026). https://doi.org/10.1016/j.devcel.2026.02.006
61. Zhang, Z.; Jones, S.; Hagood, J. S.; Fuentes, N. L.; Fuller, G. M. STAT3 acts as a co-activator of glucocorticoid receptor signaling. *J. Biol. Chem.* **272**, 30607-10 (1997). https://doi.org/10.1074/jbc.272.49.30607
62. Schneider, C. A.; Rasband, W. S.; Eliceiri, K. W. NIH Image to ImageJ: 25 years of image analysis. N*at. Methods* **9**, 671-5 (2012). https://doi.org/10.1038/nmeth.2089
63. Ito, T. et al. Cell barrier function of resident peritoneal macrophages in post-operative adhesions. *Nat. Commun.* **12**, 2232 (2021). https://doi.org/10.1038/s41467-021-22536-y
64. Glaros, E. et al. Targeting vascular adhesion protein-1 and myeloperoxidase with a dual inhibitor SNT-8370 in preclinical models of inflammatory disease. *Nat. Commun.* **16**, 3430 (2025). https://doi.org/10.1038/s41467-025-58454-6
65. Wang, Y. et al. DOT1L drives endothelial-to-mesenchymal transition and fibrotic vascular remodeling via H3K79 methylation. *Adv. Sci.* **13**, e15581 (2026). https://doi.org/10.1002/advs.202515581
66. Yu, Y. et al. Hepatic transferrin plays a role in systemic iron homeostasis and liver ferroptosis. *Blood* **136**, 726-39 (2020). https://doi.org/10.1182/blood.2019002907
67. Kaur, I. et al. Primary hepatocyte isolation and cultures: technical aspects, challenges and advancements. *Bioengineering* **10**, 131 (2023). https://doi.org/10.3390/bioengineering10020131
68. Abberbock, E. et al. A single-nucleotide enhancer mutation overrides chromosomal sex to drive XX male development. *Nat. Commun*. **17**, 3186 (2026). https://doi.org/10.1038/s41467-026-71328-9

GOLD ■ METHODS

Key resources table [Table 1]

EXPERIMENTAL MODEL AND SUBJECT DETAILS

Animals

The *Smad4*$^{fl/fl}$ mice were obtained from Dr. Chu-Xia Deng and were maintained on the 129S6/SvEvTac background. *Smad4*$^{fl/fl}$ mice were mated with Alb-Cre transgenic mice to produce hepatocytes- restricted Smad4 knockout animals (*Smad4*$^{fl/fl}$; Alb-Cre). All animals were maintained in a specific pathogen-free (SPF) facility. To induce dietary iron deficiency, 4-week-old mice received a low-iron diet (AIN-76A-diet, 0.9 mg Fe kg^{-1}, D08080402, Research Diets, Inc., New Brunswick, NJ, USA) for 4 weeks. The control (standard) diet provided 50 mg Fe kg^{-1} (AIN-76A-diet, D08080401, same supplier)[49]. In the current study, the animal experiments were performed using 8-12 week-of-age male mice. Mice were randomly allocated to experimental cohorts. For histological evaluation, slides were coded and scored by an investigator blinded to the group allocation. All animal procedures were conducted according to the guidelines for laboratory animal care and use and received approval from Laboratory Animal Welfare and Ethics Review Committee, Zhejiang University (ZJU20250797).

Animal models

In the model of infection, the mice received an intraperitoneal with *Escherichia coli* Top10 strain harboring the green fluorescent protein (GFP) gene in the Puc19 plasmid. For the supplementation of *Reg3b* and *Reg3g*, 1 μg of recombinant *Reg3b* protein (R&D systems; 5110-RG-050) and 1μg of recombinant *Reg3g* protein (R&D systems; 8189-RG-050) dissolved in 200 μL PBS were injected i.p. after infection. The control group was injected i.p. with 200 μL PBS. In the further study, mice were administered an intraperitoneal injection with 5 mg of RU486 (Mifepristone, Sigma M-8046) per 25 g in 50 μL dimethyl sulfoxide (DMSO), 30 min prior to infection, and the control group received an injection of 50 μL DMSO.

METHOD DETAILS

PCR genotyping

The Easy Tissue & Blood DNA Extraction Kit (#DR0301250, Zhejiang Easy-Do Biotech Co, Ltd) was used for animal genotyping, and tail tip biopsies were used to extract genomic DNA for PCR analysis. All the primer sequences were provided in Extended Support Table 1.

Analyses of serum

After anesthetizing mice, the blood was collected via left ventricle puncture and kept for 2 h under ambient conditions. Subsequently, the supernatant serum was harvested via centrifugation for 5,000 rpm for 10 min. The serum ALT and AST levels were measured using an enzymatic assay kit (Nanjing Jianchen, C-009-3-1; C-009-3-2), and the level of TNF-α (MTA00B; R&D systems) and IL-6 (M6000B; R&D systems) in the serum were measured by ELISA Kit.

Liver transcriptomic analysis

Genome-wide transcript levels were examined in hepatic samples collected from control mice, Smad4 LKO and Stat3 LKO mice. For each sample, 1-3 μg RNA served as the input material. These experiments were performed at Annoroad Gene Technology. The NEBNext Ultra RNA Library Prep Kit for Illumina (E7530L, New England Biolabs, Ipswich, MA) was employed to prepare the sequencing libraries in accordance with the kit manufacturer's protocol. Index-coded samples were clustered on a cBot system using the HiSeq PE Cluster Kit v4-cBot-HS (Illumina). Following cluster generation, the resulting libraries were then sequenced on a Novaseq 6000 S4 Illumina sequencing platform, and generating 150-bp paired-end reads. Raw data were subjected to quality filtering to ensure data

Table 1. Key resources table

Resource or reagent	Source	Identifier
Antibodies		
Anti-mouse CD16/32 (Clone PC61)	BioLegend	Cat# 101302; RRID: AB_302801
BV750 anti-mouse CD45-	BioLegend	Cat# 103157 RRID: AB_2734155
APCCY7 anti-mouse CD11b	Elabscience	Cat# E-AB-F1081S
BV605 anti-mouse F4/80	BioLegend	Cat# 123133 RRID: AB_2562305
Anti-mouse Ly6G-Percp-CY5.5	Elabscience	Cat# E-AB-F1108J
Anti-mouse Ly6C-APC	Elabscience	Cat# E-AB-F1121E
Anti Reg3b Antibody	R&D systems	Cat# MAB5110 RRID: AB_2178585
Anti Reg3g Antibody	Abcam	Cat# ab198216 RRID: AB_2073504
Anti-Albumin antibody	Proteintech	Cat# 16475-1-AP RRID: AB_2242567
Anti Stat3 Antibody	Cell signaling technology	Cat# 9139 RRID: AB_331757
Anti p-Stat3 Antibody	Cell signaling technology	Cat# 9145 RRID: AB_2491009
Anti-Lamin A/C antibody	Abclonal	Cat# A0249 RRID: AB_2757062
Anti Gapdh Antibody	Cell signaling technology	Cat# 5174T RRID: AB_10622025
Anti GR Antibody	Santa cruz	Cat# sc393232 RRID: AB_2687823
HRP goat anti-rabbit IgG secondary antibody	Abclonal	Cat# AS014 RRID: AB_2769854
HRP goat anti-mouse IgG secondary antibody	Abclonal	Cat# AS003 RRID: AB_2769851
Normal Rabbit IgG	Cell Signaling Technology	Cat# 2729S RRID: AB_1031062
Histone H3 (D2B12) XP Rabbit mAb	Cell Signaling Technology	Cat# 4620 RRID: AB_1904005
Anti Smad4 Antibody	Cell Signaling Technology	Cat# 38454 RRID: AB_2728776
Peptides, chemicals, and recombinant proteins		
Zombie Aqua™ Fixable Viability Kit	BioLegend	Cat# 423101
DMEM	Basal Media	Cat# L110KJ
PBS	Basal Media	Cat# B260KJ
FBS, Premium	Gibco™	Cat# A5670701
Penicillin Streptomycin	Basal Media	Cat# S110JV
L-Glutamine	Gibco™	Cat# 25030081
Sodium Pyruvate	Gibco™	Cat# 11360070
Percoll	Cytiva	Cat# 17089101
SYBR green master hybrid	Yeason	Cat# 11184ES03
Recombinant Reg3b protein	R&D system	Cat# 5110-RG-050
Recombinant Reg3g protein	R&D system	Cat# 8189-RG-050
Collagenase IV	Solarbio	Cat# C8160
AIN-76A-diet without added iron	Research diets	Cat# D08080402
AIN-76A-diet	Research diets	Cat# D08080401
RU486	Sigma	Cat# M-8046
PBS-encapsulated liposomes	Yeason	Cat# 40338ES

Clodronate liposomes	Yeason	Cat# 40337ES
Protease Inhibitor Cocktail	Sigma	Cat# P8340
5 x SDS-PAGE loading buffer	Epizyme	Cat# LT101S
Dexamethasone	MCE	Cat# HY-14648
Hydrocortisone	MCE	Cat# HY-N0583
ChIP-Grade Protein G Magnetic Beads	Cell Signaling Technology	Cat# 9006
RNAse A	Cell Signaling Technology	Cat# 7013
0.5M EDTA	Cell Signaling Technology	Cat# 7011
Micrococcal Nuclease	Cell Signaling Technology	Cat# 10011
Recombinant mouse IL-6	Peprotech	Cat# 216-16-10UG
Recombinant mouse Activin A	Peprotech	Cat# PHC9564
Recombinant Mouse BMP4	Peprotech	Cat# 315-27-10UG
RBC lysis buffer	BioLegend	Cat# 420302
Commercial assays		
Mouse TNF-alpha Quantikine ELISA Kit	R&D system	Cat# MTA00B
Mouse IL6 Quantikine ELISA Kit	R&D system	Cat# M6000B
Easy Tissue&Blood DNA extraction kit	Easy-Do Biotech	Cat# DR0301250
PrimeScript RT reagent Kit	Takara	Cat# RK014B
Pierce™ ECL Weste129S6/SvEvTacrn Blotting Substrate	ThermoFisher Scientific	Cat# 32106
Simple ChIP Plus Enzymatic Chromatin IP Kit	Cell Signaling Technology	Cat# 9005S
Alanine aminotransferase Assay Kit	Nanjing Jianchen	Cat# C-009-3-1
Aspartate aminotransferase Assay Kit	Nanjing Jianchen	Cat# C-010-3-1
Minute Cytoplasmic and Nuclear Extraction Kit	Invent Biotechnologies	Cat# SC-003
Serum iron/TIBC kit	Point scientific	Cat# I7506
Experimental models: Organisms/strains		
Mouse: 129S6/SvEvTac /*Smad4*$^{fl/fl}$ (CD45.2)	Kind gifted from Dr. Chuxia Deng	N/A
Albumin-cre mice	GemPharmatech	GemPharmatech # T055035
B6.C57BL/6JGpt (CD45.2)	GemPharmatech	GemPharmatech # N000013
Oligonucleotides (Sequences of the primers used for genotyping)		
See Extended Support Table 1 for primers used for Chip-PCR in this study	This Study	N/A
Oligonucleotides (Sequences of the primers used for Chip-PCR)		
See Extended Support Tables 2 and 3 for primers used for qRT-PCR in this study	This Study	N/A
Oligonucleotides (Sequences of the primers used for qRT-PCR)		
See Extended Support Table 4 for primers used for qRT-PCR in this study	This Study	N/A
Software and algorithms		
ImageJ	Schneider et al.[62]	https://imagej.nih.gov/ij/
Flowjo	BD Sciences	Version 10.8.1
GraphPadSoftware	GraphPadPrism	https://www.graphpad.com/scientific-software/prism
ImageLab	Bio-Rad	https://www.biorad.com/en-us/product/image-lab-software?ID=KRE6P5E8Z
Adobe illustrator	Adobe	https://www.adobe.com/cn/creativecloud/roc/business.html

GR: Glucocorticoid receptor; HRP: horseradish peroxidase; IgG: immunoglobulin G; DMEM: Dulbecco's Modified Eagle's Medium; PBS: phosphate buffered saline; FBS fetal bovine serum; RU486: mifepristone; SDS-PAGE: sodium dodecyl sulfate-polyacrylamide gel electrophoresis; RBC: red blood cell; TNF: tumor necrosis factor; BMP4: bone morphogenetic protein 4; TIBC: total iron-binding capacity; RT-PCR: reverse transcription polymerase chain reaction; ChIP: chromatin immunoprecipitation.

quality for further analysis. The National Center for Biotechnology Information (NCBI) database provided the information regarding the mus musculus reference genome and gene annotations.

For the genome-wide transcriptional profiles of liver tissues from WT *vs.* WT + *E. coli*, WT + *E. coli vs.* WT + RU486 mice, total RNA was isolated with TransZol up (TransGen Biotech) according to the supplier's protocol, and RNA quality and yield were evaluated using a NanoDrop spectrophotometer. Library preparation was performed employing the VAHTS Universal V8 RNA-seq Library Prep Kit for Illumina according to the manufacturer's protocol. Library concentrations were measured using a Qubit 4.0 fluorometer (Thermo Fisher, USA), and libraries were then sequenced on the platform of Illumina Novaseq with a paired-end 150 bp (PE150) read length. Raw reads were filtered using fastp (v0.20.1) to remove adapter sequences, trim low-quality bases, and . Filtered reads were mapped onto the the Mus musculus reference genome (obtained from the NCBI database). Expression differences were assessed via edgeR based on a negative binomial model, and significant differentially expressed genes (DEGs) were identified by applying thresholds of FDR < 0.05 together with |log2FC| ≥ 1. Using clusterProfiler (v4.0.2) with Fisher's exact test, we then carried out GO and KEGG pathway enrichment analyses.

In vivo depletion of macrophage

The depletion of macrophages was achieved via intraperitoneal administration of clodronate liposomes (200 µL per mouse, Yeason, 40337ES)[63]. PBS-encapsulated liposomes (Yeason, 40338ES) were administered in an analogous manner as a control. The macrophage depletion efficacy was evaluated using F4/80 antibody at 48 h after treatment by flow cytometry.

Macrophage-killing assays

In the bacterial killing assay, peritoneal macrophages elicited by thioglycollate were exposed to TOP10 *E. coli* strain for 20 min. Subsequently, these cells were rinsed using PBS (to eliminate extracellular bacteria), maintained in DMEM containing 100 µg/mL gentamycin for 20 min (to destroy remaining external bacteria), followed by another 120-min incubation in DMEM with 25 µg/mL gentamycin. The CFU counts were subsequently quantified from macrophages lysates[49].

Collection and culture of peritoneal macrophages (PMs)

Macrophages were cultured in complete DMEM containing 10% FBS along with 100 U/mL penicillin/streptomycin. To obtain PMs, mice received an intraperitoneal injection of 1 mL of sterile 4% thioglycollate[64]; The PMs were harvested 60 h later.

Chromatin immunoprecipitation (ChIP) assay

The liver tissues were collected from control mice, *E. coli*-infected control mice and *E. coli*-infected LKO mice. Chromatin immunoprecipitation was carried out utilizing the Simple ChIP Plus Enzymatic Chromatin IP Kit (#9005; Cell Signaling Technology) following the manufacturer's protocol[65]. Immunoprecipitation was conducted with using magnetic beads and antibodies targeting Smad4 (38454, Cell Signaling Technology), p-Stat3 (9145, Cell Signaling Technology), GR (sc-393232, Santa Cruz biotechnology) as well as anti-IgG antibodies. The recovered DNA fragments were then directly employed for quantitative RT-PCR analysis using primers specific to the *Reg3b* and *Reg3g* promoter regions [Extended Support Tables 2 and 3].

Measurements of tissue non-heme iron

The measurements were finished as previously described[66]. Mouse organ biopsies were weighed, then digested for 72 h using a prepared acid solution. During this period, vortexed the sample every day. The samples were centrifuged after full digestion and then the reaction was carried out by adding the prepared color solution and the absorbance was measured. The iron content of liver and serum was measured after infection. The data was presented as micrograms of iron per gram wet weight of tissue.

Assessment of bacterial CFU

Serial blood dilutions or peritoneal washes from mice were spread onto LB agar plates. Hepatic bacterial burdens were assessed by collecting a 100-mg liver sample, homogenized in 1 mL of sterile PBS, and then serial dilutions were cultured on LB plates. Colony count was performed at 37 °C for 24 h, and CFU/organ was calculated.

Isolation and culture of primary hepatocytes

A collagenase perfusion combined with density gradient centrifugation was employed to harvest primary hepatocytes from control and *Smad4 LKO* mice[67]. Briefly, animals were anesthetized and perfused through the portal vein with 1× perfusion buffer, followed by 1× digestion buffer. Following perfusion, the liver was excised and passed through a 70-µm cell strainer. The cell suspension was centrifuged at 500 × *g* for 1 min, and primary hepatocytes were resuspended in a mixture containing 5 mL Dulbecco's modified Eagle medium (DMEM; BasalMedia, Shanghai), 0.5 mL 10 × PBS (BasalMedia, B260KJ), and 4.5 mL Percoll (Cytiva, Shanghai, 17089101). Subsequently, the cells were purified by density gradient centrifugation at 600 rpm for 10 min at 4 °C. The purified primary hepatocytes were then cultured in DMEM supplemented with 10% FBS (Gibco, 10100147C) and 1% penicillin-streptomycin (BasalMedia, S110JV) in a humidified atmosphere containing 5% CO_2 at 37 °C.

Real-time PCR

Total RNA was extracted from cells or tissues with reagent of TRIzol (Invitrogen, Carlsbad, USA) following the protocol, and RNA concentration was measured using spectrophotometer (Thermo NANODROP 2000). Using the PrimeScript RT kit (RR014B,Takara), RNA was converted to cDNA in accordance with the manufacturer's instructions, followed by qRT-PCR using power supply SYBR green master hybrid (Yeasen, China; 11184ES03). Quantitative PCR was carried out employing the two-step RT-qPCR method, and triplicate samples were run on the Roche LightCycler® 480 II (Roche, Shanghai, China). For each target gene, its expression level was normalized to that of a corresponding control gene (Hprt or Actin), as well as the the $2^{-\Delta\Delta Ct}$ approach was used for quantification analysis[68]. The primers applied in qRT-PCR are shown in Extended Support Table 4 for supporting information.

Flow cytometric analysis

Single-cell suspensions from liver, peritoneal fluid and blood were stained on ice for 30 min with following antibodies: anti-mouse CD16/32 Antibody (Biolegend, Cat#101302), anti-mouse CD45-BV750 (Biolegend, Cat#103157), anti-mouse CD11b-APCCY7 (Elabscience, E-AB-F1081S), anti-mouse F4/80-BV605 (Biolegend; Cat#123133), anti-mouse Ly6G-Percp-CY5.5 (Elabscience, E-AB-F1108J), anti-mouse Ly6C-APC (Elabscience, E-AB-F1121E) and anti-mouse L/D-Amcyan (Biolegend, Cat#423101). The antibody used for FACs sorting and analysis are listed in Extended Support Table 5.

Within myeloid-lineage leukocytes, neutrophils are stained as $CD45^+CD11b^+Ly6G^+$, macrophages are stained as $CD45^+$ $F4/80^+CD11b^+$(Ly6G negative), and monocyte are stained as $CD45^+CD11b^+Ly6G$-F4/80- or $CD45^+CD11b^+Ly6G$-$Ly6C^+$. Flow cytometry was performed with a BD Fortessa cytometer (BD Biosciences, San Jose, CA). The resulting data acquisition and analysis are completed by the use of Flow Jo software. The cell number was counted by ACEA Novocyte (TM) flow cytometer. For calculation of the total parenchymal cell number in liver, samples were normalized to the weight

of liver. The total cell count in the blood and peritoneal fluid for each cell population was derived through multiplying the total cell count by the proportion of events falling within each specific gate. Flow cytometry data were acquired and analyzed without knowledge of the sample group assignments.

Protein extraction and immunoblotting analysis

Cellular lysate containing radio immunoprecipitation assay (RIPA) and protease inhibitor cocktail (Sigma, P8340) was used to extract total protein from cells. The homogenate was spun at 12,000 rpm for 5 min at 4 °C. Supernatant was collected and mixed with 5 × sodium dodecyl sulfate-polyacrylamide gel electrophoresis (SDS-PAGE) buffer (Epizyme, LT101S). In the next step, these protein samples were then loaded onto SDS-PAGE gel, subjected to electrophoresis (80 V constant voltage, 90 min) and transfer (300 mA constant current, 90 min) using transfer apparatus (Bio-rad). After blocking with 5% non-fat milk in Tris-buffered saline with Tween-20 (TBST) for 1 hour, the membrane was incubated with the primary antibody at 4 °C overnight, followed by three washes (10 min each with TBST). Further the horseradish peroxidase (HRP)-conjugated secondary antibody was used to incubate the membranes for 1 h at room temperature, followed by three washes with TBST, each lasting 10 min. Lastly the membranes were detected on ChemiDoc XRS + Chemiluminescent imaging systems (Bio-Rad, United States) using FDbio-Pico FD8000 enhanced chemiluminescence (FDbio science, Hangzhou, China). We have provided the details of primary and secondary antibodies employed in Western blot analysis below: anti-*Reg3b* antibody (MAB5110, R&D systems), anti-*Reg3g* antibody (ab198216, 1:1000, Abcam), anti-Albumin antibody (16475-1-AP, 1:1000, proteintech), anti-stat3 antibody (9139, 1:1000, Cell signaling technology), anti p-stat3 antibody (1:1000, 9145, Cell signaling technology), anti-Lamin A/C antibody (A0249, 1:1000, Abclonal), anti-Gapdh antibody (5174T, 1:1000, CST), and anti-GR antibody (sc393232, 1:1000, Santa-Cruz), HRP goat anti-rabbit IgG secondary antibodies (AS014, 1:2000, ABclonal), HRP goat anti-mouse IgG secondary antibodies (AS003, 1:2000 dilution, ABclonal).

QUANTIFICATION AND STATISTICAL ANALYSIS

All statistical calculations were carried out with GraphPad Prism 9.0, and summary data are shown as the mean ± SD. Data were analyzed using unpaired t-test (for two-group comparisons), one-way ANOVA or two-way ANOVA (for multi-group comparisons). Survival curves were evaluated using the log-rank (Mantel-Cox) test. A P-value < 0.05 was deemed statistically significant. Significance levels were denoted as $^{*}P < 0.05$, $^{**}P < 0.01$, $^{*}P < 0.001$, and N.S. (not significant, $P > 0.05$).

EXTENDED SUPPORT MATERIALS

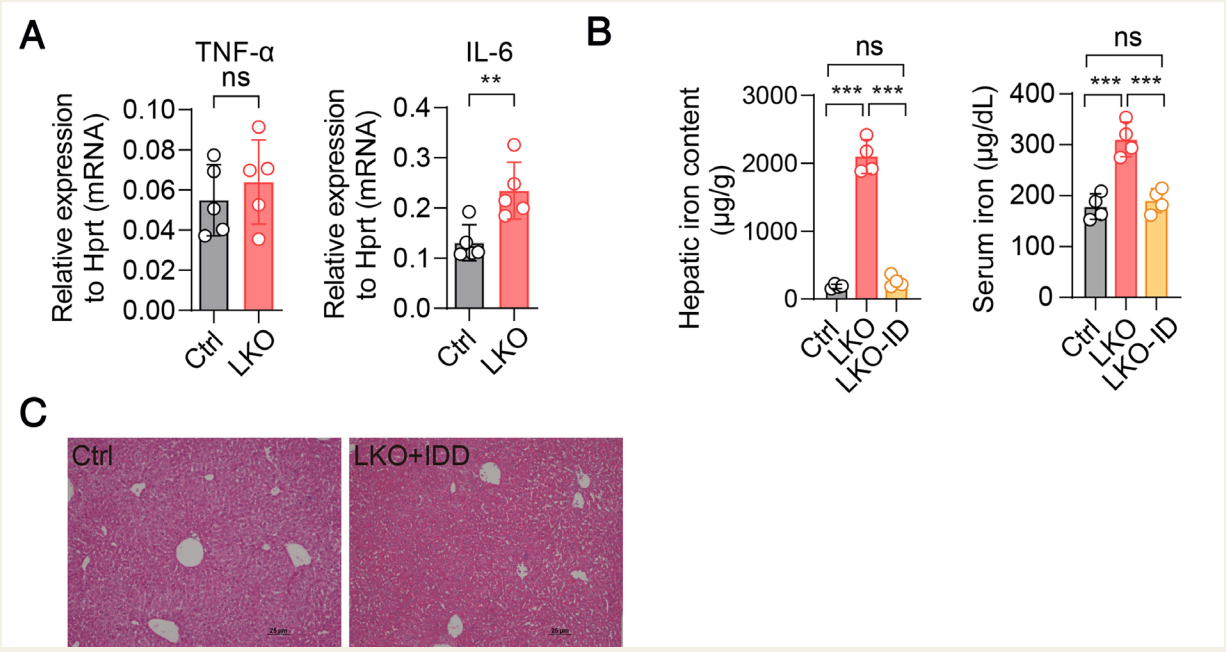

Extended Support Figure 1. Iron overload was not the major factor for the susceptible of LKO mice to bacterial infection.

(A) The mRNA level of TNF-α and IL-6 in the liver of control (n = 5) and LKO mice (n = 5) 12 h post *E. coli* infection; (B) The iron level in the liver and serum of Control, LKO and LKO + ID mice (n = 4); (C) Representative hematoxylin and eosin staining of histological sections of liver tissue in control and LKO + ID mice 12 h post infection. Circles correspond to individual mouse. Results are represented as mean ± SD. P values in (A) were determined using unpaired Student's t-tests. P values in (B) were determined using one-way ANOVA. $^{*}P < 0.05$; $^{**}P < 0.01$; $^{***}P < 0.001$. NS: Not significant; TNF-α: tumor necrosis factor-alpha; IL-6: interleukin-6; LKO: liver-specific Smad4 knockout; *E. coli: Escherichia coli.*

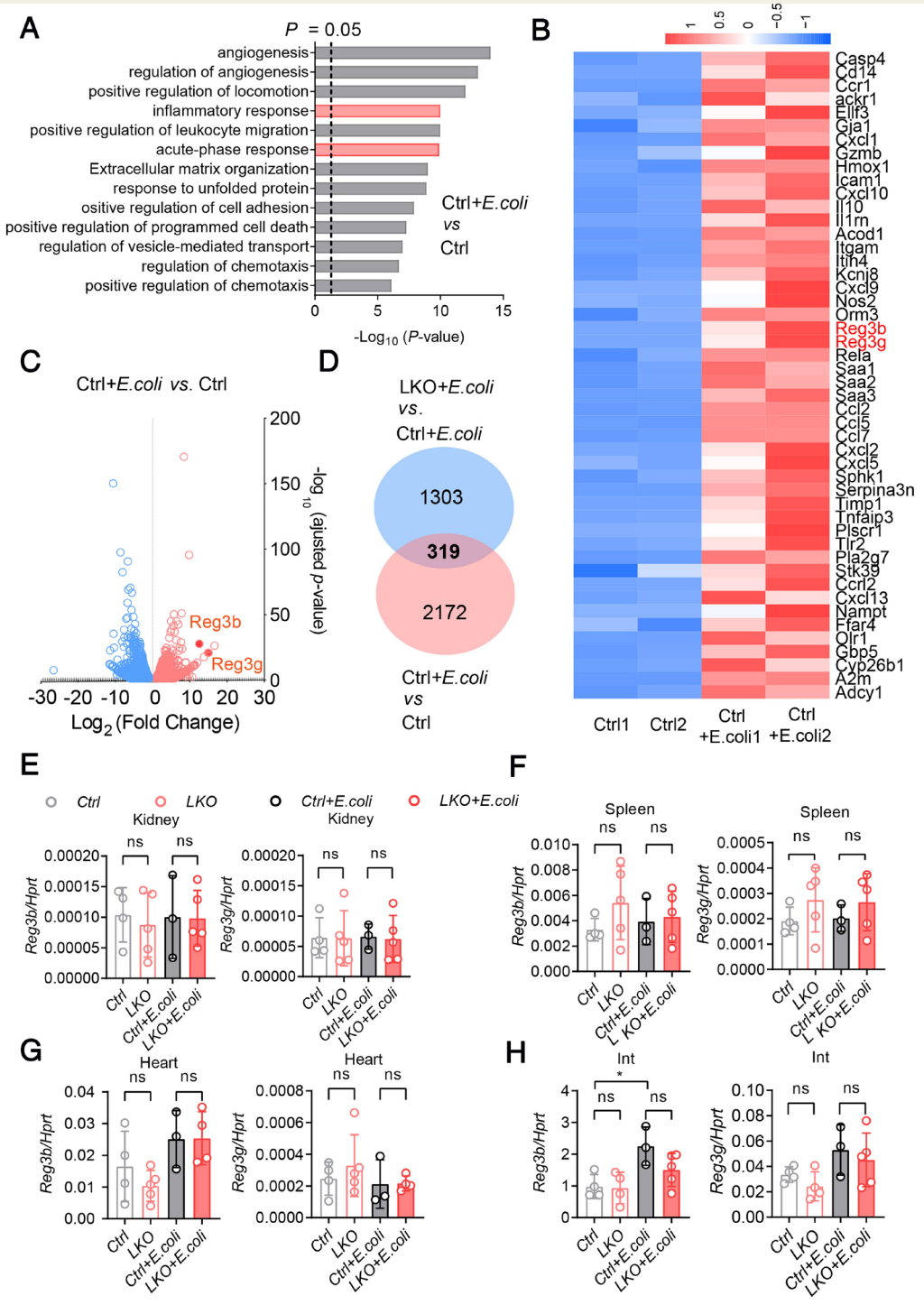

Extended Support Figure 2. The expression of *Reg3b* and *Reg3g* is upregulated upon *E. coli* infection.
(A) Go analysis of differentially expressed genes (upregulated) in the liver from Ctrl + *E. coli* and Ctrl mice; (B) Heat map representation of differentially upregulated genes in the inflammatory response pathway (Ctrl + *E. coli* group *vs.* Ctrl group); (C) Volcano plot representation of RNA sequencing data of genes upregulated (red) or downregulated (blue) in the liver from Ctrl + *E. coli* and Ctrl mice; (D) The venn diagram showing the number of differentiated expressed genes in LKO + *E. coli vs.* Ctrl + *E. coli* group and Ctrl + *E. coli vs.* Ctrl group; (E) The mRNA level of *Reg3b* and *Reg3g* in the kidney of control and LKO mice (non-infected and 12 h post *E. coli* infection, respectively) (n = 3-5 per group); (F) The mRNA level of *Reg3b* and *Reg3g* in the spleen of control and LKO mice (non-infected and 12 h post *E. coli* infection, respectively) (n = 3-5 per group); (G) The mRNA level of *Reg3b* and *Reg3g* in the heart of control and LKO mice (non-infected and 12 h post *E. coli* infection, respectively) (n = 3-5 per group); (H) The mRNA level of *Reg3b* and *Reg3g* in the intestine of control and LKO mice (non-infected and 12 h post *E. coli* infection, respectively) (n = 3-5 per group). Circles correspond to individual mouse. Results are represented as mean ± SD. The P values in (C) were deter-mined using unpaired Student's t-tests. $^{*}P < 0.05$; $^{**}P < 0.01$; $^{***}P < 0.001$. LKO: Liver-specific Smad4 knockout; *E. coli*: *Escherichia coli*.

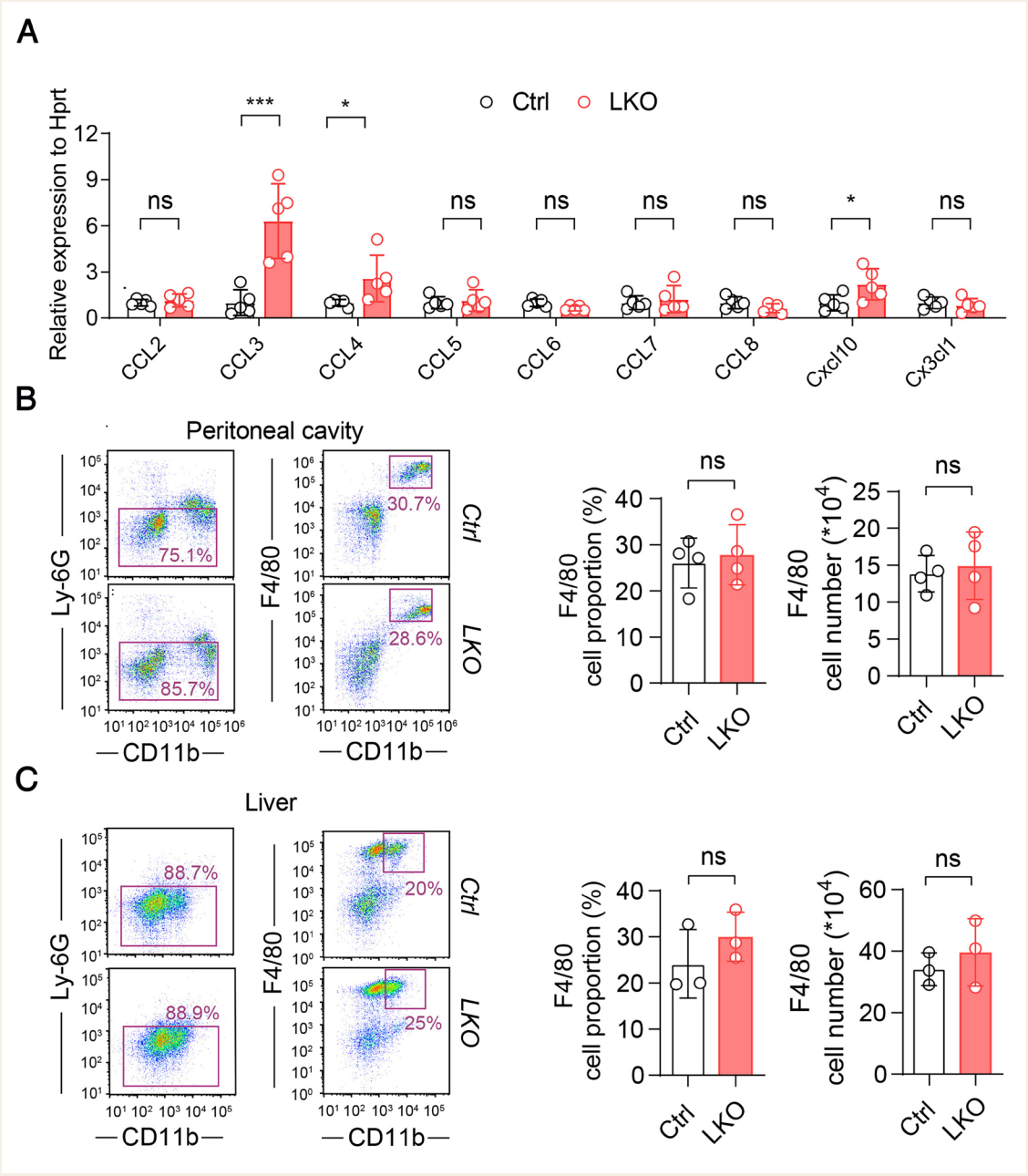

Extended Support Figure 3. Hepatic Smad4 deficiency do not affect the number of macrophages at non-infected conditions.
(A) The mRNA levels of several chemokines (*Ccl2, Ccl3, Ccl4, Ccl5, Ccl6, Ccl7, Ccl8, Cxcl10, Cx3cl1*; quantified by RT-PCR) in the liver of control (n = 5) and LKO mice (n = 5) 12 h post *E. coli* infection; (B) Representative flow cytometry dot plot and corresponding proportion and cell number of macrophages in the peritoneal fluid from control (n = 4) and LKO (n = 4) mice; (C) Representative flow cytometry dot plot and corresponding proportion and cell number of macrophages in the liver from control (n = 3) and LKO (n = 3) mice. Circles correspond to individual mouse. Results are represented as mean ± SD and are obtained at embryonic day 16.5. The P values in (A-C) were determined using unpaired Student's t-tests. $^{*}P < 0.05$; $^{**}P < 0.01$; $^{***}P < 0.001$. NS: not significant; LKO: liver-specific Smad4 knockout; *E. coli*: *Escherichia coli.*

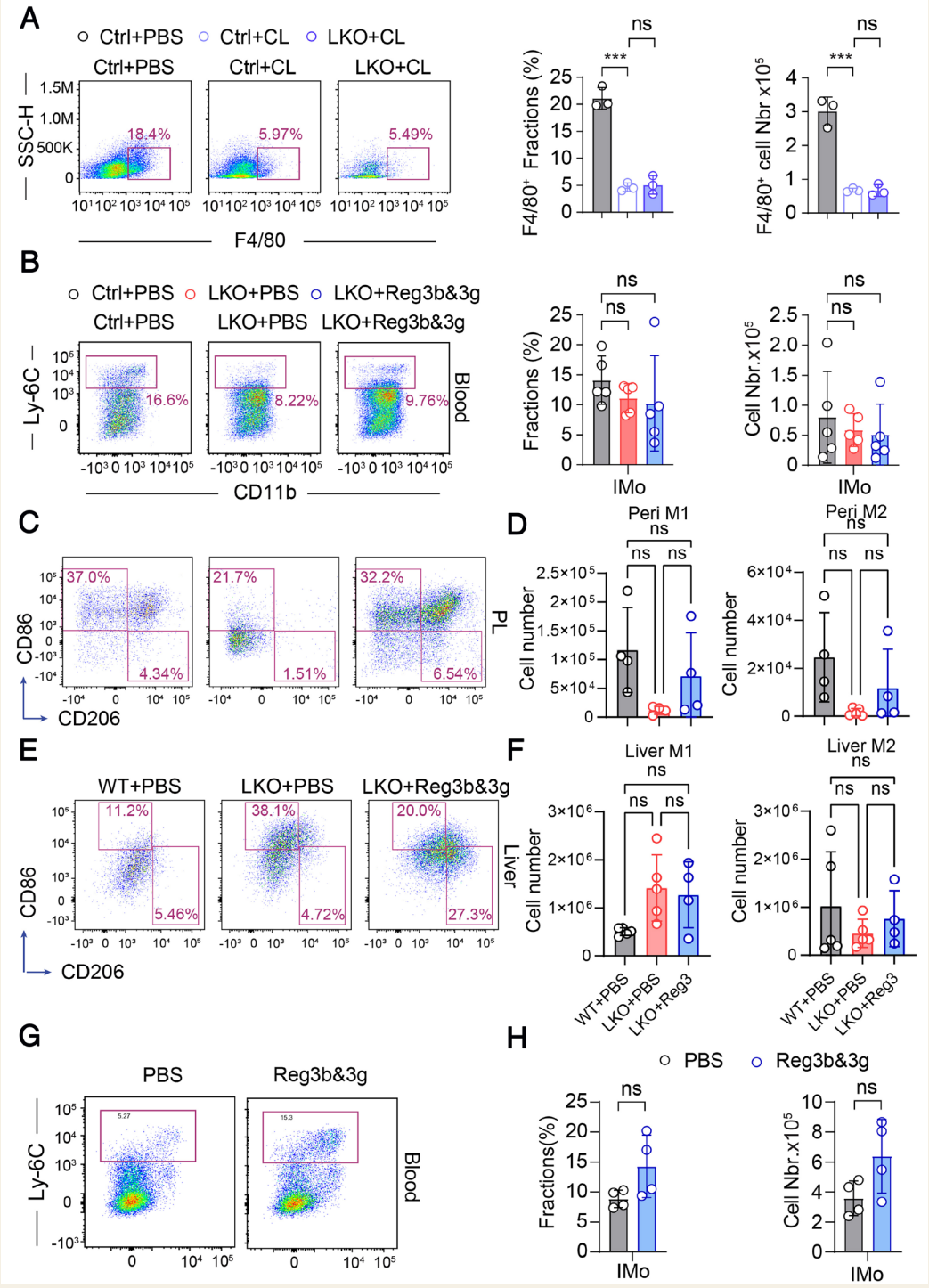

Extended Support Figure 4. *Reg3b* and *Reg3g* exert anti-bacterial activity through recruitment of macrophages.
(A) Representative flow cytometry dot plot and corresponding proportion and cell number of F4/80$^+$ cells in the peritoneal fluid from control, LKO + PBS and LKO + clodronate liposomes mice 48 h post infection; (B) Representative flow cytometry dot plot and corresponding propor-tion and cell number of inflammatory monocytes in the blood from control, LKO + PBS, LKO + rReg3b and rReg3g mice; (C) The corresponding flow cytometry dot plot and cell number of M1 and M2 macrophages in the peritoneal fluid of control, LKO + PBS and LKO + rReg3b and rReg3g mice (n = 4-5 per group); (D) The corresponding flow cytometry dot plot and cell number of M1 and M2 macrophages in the liver of control, LKO + PBS and LKO + rReg3b and rReg3g mice (n = 4-5 per group); (E) Representative flow cytometry dot plot of monocytes in the blood and liv-er of WT + PBS and WT + rReg3b and rReg3g mice; (F) The cell number of inflammatory monocytes in the blood of WT + PBS and WT + rReg3b and rReg3g mice. Circles correspond to individual mouse. Results are represented as mean ± SD. The P values in (A and B) were determined us-ing one-way ANOVA. The P values in (D-F) were determined using unpaired Student's t -tests. The P values in (E) were determined using two-way ANOVA. $^*P < 0.05$; $^{**}P < 0.01$; $^{***}P < 0.001$. LKO: Liver-specific Smad4 knockout; PBS: phosphate buffered saline; WT: wild type.

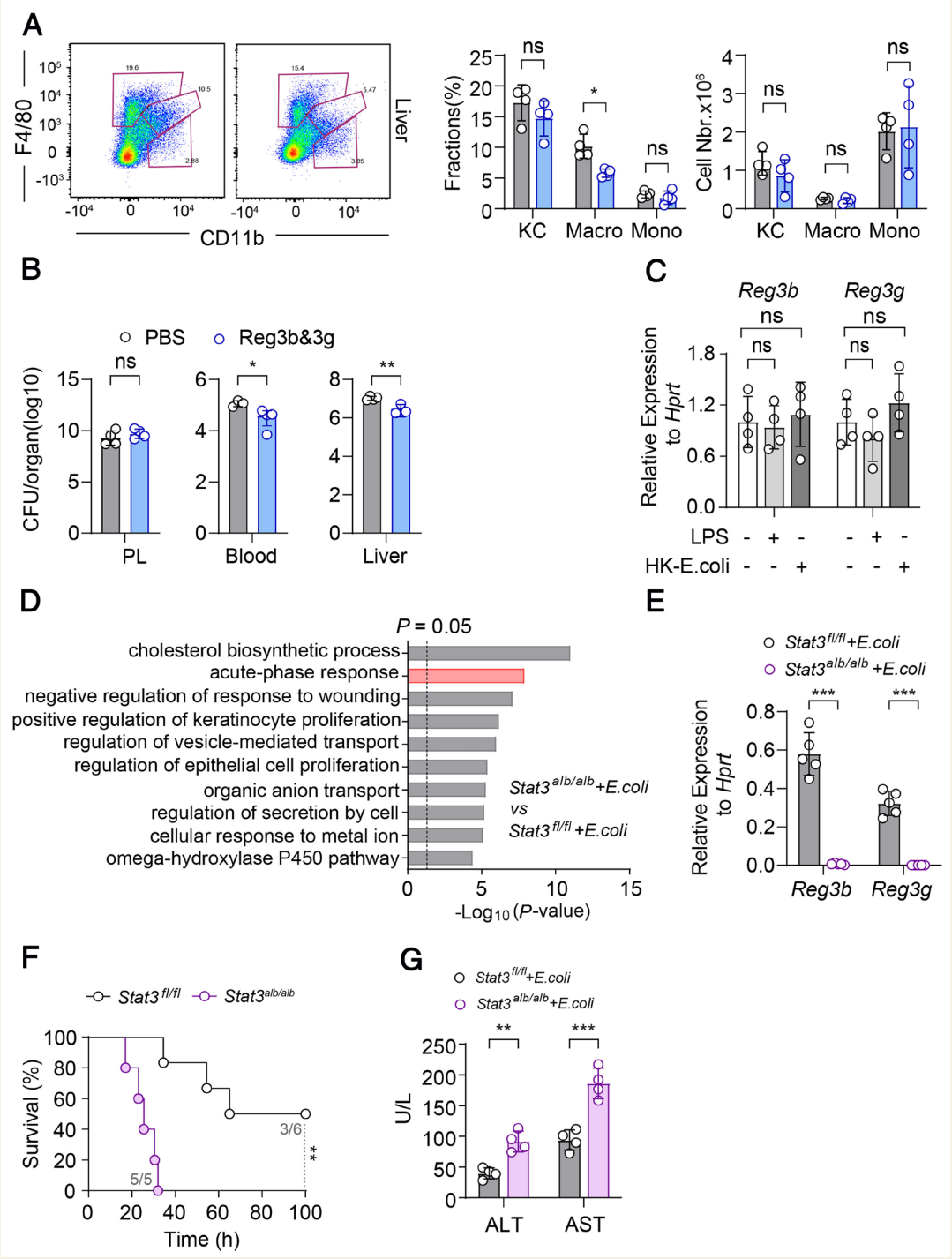

Extended Support Figure 5. Hepatic stat3 deficiency resulted in decreased *Reg3b* and *Reg3g* expression upon infection.
(A) The corresponding proportion and cell number of immnue cells (kuffer cells, macrphages and monocytes) in the liver of WT + PBS and WT + rReg3b and rReg3g mice; (B) The bacterial CFU counts measured in the peritoneal fluid, blood and liver of WT + PBS and WT + rReg3b and rReg3g mice 12 h post infection; (C) The mRNA levels of *Reg3b* and *Reg3g* measured in primary hepatocytes isolated from control and LKO mice and treated with LPS or heat-killed *E. coli* (HK-*E. coli*); (D)Go analysis of differentially expressed genes (downregulated) in the liver from $Stat3^{fl/fl}$ and $Stat3^{fl/fl}$; Alb-cre ($Stat3^{alb/alb}$) mice 12 h post infection; (E) The mRNA level of *Reg3b* and *Reg3g* in the liver of $Stat3^{fl/fl}$ (n = 5) and $Stat3^{alb/alb}$ mice (n = 5) 12 h post infection; (F) Kaplan-Meier survival curve of $Stat3^{alb/alb}$ mice (n = 5) and $Stat3^{fl/fl}$ mice (n = 6) following an i.p. injection of *E. coli*; (G) Serum ALT and AST levels of $Stat3^{fl/fl}$ (n = 4) and $Stat3^{alb/alb}$ mice (n = 4) were measured 12 h post infection. Circles correspond to individual mouse. Results are represented as mean ± SD. P values in (A) were determined using one-way ANOVA. P values in (C) were determined using unpaired Student's t-tests. $^{*}P < 0.05$; $^{**}P < 0.01$; $^{***}P < 0.001$. NS: Not significant; LKO: liver-specific Smad4 knockout; PBS: phosphate buffered saline; WT: wild type; CFU: colony forming unit; LPS: lipopolysaccharide; ALT: alanine aminotransferase; AST: as-partate aminotransferase; *E. coli: Escherichia coli.*

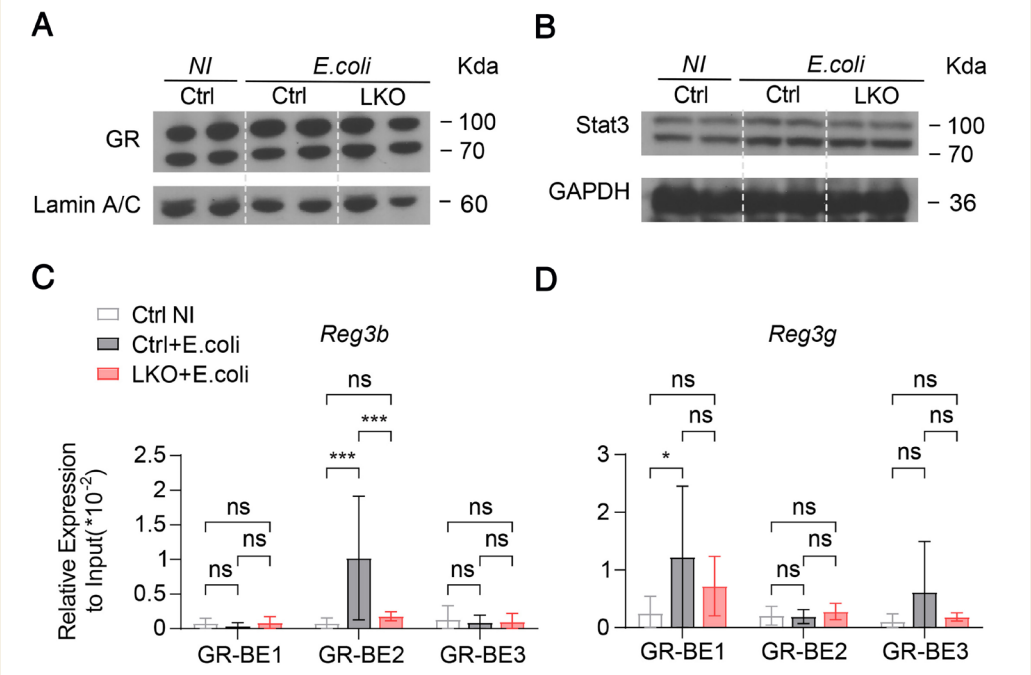

Extended Support Figure 6. Smad4 regulated the expression of *Reg3b* and *Reg3g* via GR.
(A) Western blot analysis of Stat3 protein in the liver tissues of non-infected control mice, *E. coli* infected control mice and *E. coli* infected LKO mice; (B) Western blot analysis of Glucocorticoid Receptor protein in the liver tissues of non-infected control mice, *E. coli* infected con-trol mice and *E. coli* infected LKO mice; (C) ChIP assay using GR antibody followed by qPCR of the *Reg3b* promoter (GR-BE1, GR-BE2) in the liver of non-infected control mice, *E. coli* infected control mice and *E. coli* infected LKO mice; (D) ChIP assay using GR antibody followed by qPCR of the Reg3g promoter (GR-BE1, GR-BE2) in the liver of non-infected control mice, *E. coli* infected control mice and *E. coli* infected LKO mice. Circles correspond to individual mouse. Results are represented as mean ± SD. The P values in (C and D) were determined using one-way ANOVA. $^{*}P < 0.05$; $^{**}P < 0.01$; $^{***}P < 0.001$. NS: not significant; ChIP: chromatin immunoprecipitation; GR: glucocorticoid receptor; qPCR: quantitative polymerase chain reaction; LKO: liver-specific Smad4 knockout; *E. coli*: *Escherichia coli*.

Extended Support Table 1. Sequences of the primers used for genotyping PCR analyses

Gene	Forward primers	Reverse primers
Smad4	GGGCAGCGTAGCATATAAGA	GACCCAAACGTCACCTTCAG
Alb-cre	GCAAACATACGCAAGGGATT	AGGCAAATTTTGGTGTACGG

Extended Support Table 2. Sequences of the primers used for ChIP analysis of the mouse *Reg3b* promoter

Gene	Forward primers	Reverse primers
mReg3b-Smad4-1	AAAGCAAGAAAGTAATCCCTCA	AGGAAAAGTAATTGTTGCTTCGTA
mReg3b-Smad4-2	ACACCTACAATTTTTAATCTGCTCA	TCAATTTGGAAAAACCTCACTTGT
mReg3b-Stat3-1	AGGTAAAGCAGGTCGGCTAA	TGAGGGAGGGACATCGTAGTA
mReg3b-Stat3-2	AATTTGTGCCCCAATGTTGCC	TTAGCCGACCTGCTTTACCTC
mReg3b-GR-1	CCCAATGTTGCCATTGTTTGC	TTAGCCGACCTGCTTTACCTC
mReg3b-GR-2	GTAAAGCAGGTCGGCTAACG	CAGCATTTGGCACAGACTCAA
mReg3b-GR-3	AGGTAAAGCAGGTCGGCTAA	AGCATTTGGCACAGACTCAA

ChIP: Chromatin immunoprecipitation.

Extended Support Table 3. Sequences of the primers used for ChIP analysis of the mouse *Reg3g* promoter

Gene	Forward primers	Reverse primers
mReg3g-Smad4-1	GAGGATGTGCCTAATCCTATAGG	ACCCAGACTCTCTCCCTCATT
mReg3g-Smad4-2	GAAACGTGAACTCCTTTCTGCC	GTGTGCTTTAGCATTAATCCATCC
mReg3g-Smad4-3	ATGAAAACTACGTCAAAGCCATTC	TGCCTCTCTGTGGGAAAGTTG
mReg3g-Stat3-1	GAGGCAGCAGGAAAGCAAGT	TGATGGTCGTGAATTAGCTGAAAG
mReg3g-Stat3-2	GCATTGTGACAAAAATACCCTGTTA	TTGAACTTTCCCCATCTTTTCCC
mReg3g-Stat3-3	CTGCTAACAGGAAAGGGCCA	TGCTCATGCAAGTCAGGGAG
mReg3g-GR-1	TGGCATCCTTAGAGCTTCAGAG	AGGTGTTAAAGTGCTGAGGTACA
mReg3g-GR-2	GCATCCTTAGAGCTTCAGAGAC	TGTCCCCAACTTAAAAGAGTCA
mReg3g-GR-3	ACAGGCAGAATGTATGGAAGGAA	TGCCACAATCCAAACCTGTCT

ChIP: Chromatin immunoprecipitation.

Extended Support Table 4. Sequences of the primers used for RT-PCR and plasmid construction

Gene	Primers for RT-PCR	Reference
Hprt-F	TTTCCCTGGTTAAGCAGTACAGCCC	Nomura *et al.*, 2016[69]
Hprt-R	TGGCCTGTATCCAACACTTCGAGA	
Gapdh-F	ATCATCCCTGCATCCACT	Adedoyin *et al.*, 2018[70]
Gapdh-R	ATCCACGACGGACACATT	
Reg3b-F	GAGGCCTGGAGGACACCTCGT	Lörchner *et al.*, 2015[71]
Reg3b-R	TTGTCCCTTGTCCATGATGCTCTTC	
Reg3g-F	TTCCTGTCCTCCATGATCAAAA	Ito *et al.*, 2017[72]
Reg3g-R	CATCCACCTCTGTTGGGTTCA	
TNF-α-F	GGCAGGTCTACTTTGGAGTCATTGC	Dube *et al.*, 2001[73]
TNF-α-R	ACATTCGAGGCTCCAGTGAATTCGG	
Il6-F	CTGGTGACAACCACGGCCTTCCCTA	Liu *et al.*, 2006[74]
Il6-R	ATGCTTAGGCATAACGCACTAGGTT	
CCl2-F	CACCTGCTGCTACTCATTCAC	Huang *et al.*, 2007[75]
CCl2-R	CACTGTCACACTGGTCACTCCTAC	
CCl3-F	TGAATGCCTGAGAGTCTTGG	Ma *et al.*, 2021[76]
CCl3-R	TTGGCAGCAAACAGCTTATC	
CCl4-F	TCTGCGTGTCTGCCCTCTC	Fine *et al.*, 2003[77]
CCl4-R	TGCTGAGAACCCTGGAGCA	
CCl5-F	GTTATGGGAGGGCTCTGGTG	Fine *et al.*, 2003[77]
CCl5-R	CCTAAGCACCAGCTCTGCG	
CCl7-F	GCGTGCATCATTGAGAAAGGA	Lee *et al.*, 2009[78]
CCl7-R	ATGGCAGTGCTCTGTGATGT	
CCl8-F	GCTACGAGAGAATCAACAATATCCAGT	Marinkovic *et al.*, 2006[79]
CCl8-R	CAGAGAGACATACCCTGCTTGGT	
Cxcl10-F	GGAGATGAGCTAGGATAGGATAGAGGG	Makuch *et al.*, 2022[80]
Cxcl10-R	TGCCCATTTTCCCAGGACCG	
Cx3cl1-F	ACGAAATGCGAAATCATGTGC	Liu *et al.*, 2025[81]
Cx3cl1-R	CTGTGTCGTCTCCAGGACAA	

Extended Support Table 5. Antibody and fluorescent labels used for FACS sorting and analysis

Antigen	Fluorochrome	Company	Clone	Catalog
CD45	BV750	Biolegend	30-F11	103157
F4/80	BV605	Biolegend	BM8	123133
CD11b	APC-CY7	Elabscience	M1/70	E-AB-F1081S
Ly-6C	APC	Elabscience	Monts 1	E-AB-F1121E
Ly-6G	PerCP-Cy5.5	Elabscience	1A8	E-AB-F1108J
LD	Amcyan	Biolegend	D7	423101
CD16/32	PerCP-Cy5.5	Biolegend	93	101302

EXTENDED SUPPORT REFERENCES

69. Nomura, M.; et al. Fatty acid oxidation in macrophage polarization. *Nat. Immunol.* **17**, 216-217 (2016). https://doi.org/10.1038/ni.3366
70. Adedoyin, O.; et al. Heme oxygenase-1 mitigates ferroptosis in renal proximal tubule cells. *Am. J. Physiol. Renal Physiol.* **314**, F702-14 (2018). https://doi.org/10.1152/ajprenal.00044.2017
71. Lörchner, H.; et al. Myocardial healing requires Reg3β-dependent accumulation of macrophages in the ischemic heart. *Nat. Med.* **21**, 353-62 (2015). https://doi.org/10.1038/nm.3816
72. Ito, T. ;et al. Il-22 induces reg3γ and inhibits allergic inflammation in house dust mite-induced asthma models. *J Exp. Med.* **214**, 3037-50 (2017). https://doi.org/10.1084/jem.20162108
73. Dube, P. H.; Revell, P. A.; Chaplin, D. D.; Lorenz, R. G.; Miller, V. L. A role for Il-1 alpha in inducing pathologic inflammation during bacterial infection. *Proc Natl. Acad Sci U S A.* **98**, 10880-5 (2001). https://doi.org/10.1073/pnas.191214498
74. Liu, D. F.; Wei, W.; Song, L. H. Upregulation of TNF-alpha and Il-6 mrna in mouse liver induced by bacille Calmette-Guerin plus lipopolysaccharide. *Acta. Pharmacol. Sin.* **27**, 460-8 (2006). https://doi.org/10.1111/j.1745-7254.2006.00301.x
75. Huang, B.; et al. CCL2/CCR2 pathway mediates recruitment of myeloid suppressor cells to cancers. *Cancer Lett.* **252**, 86-92 (2007). https://doi.org/10.1016/j.canlet.2006.12.012
76. Ma, D.; Qiao, L.; Guo, B. Smad7 suppresses melanoma lung metastasis by impairing Tregs migration to the tumor microenvironment. *Am. J. Transl. Res.* **13**, 719-31 (2021). https://pubmed.ncbi.nlm.nih.gov/33594321/
77. Fine, J. S.; et al. Impairment of leukocyte trafficking in a murine pleuritis model by IL-4 and IL-10. *Inflammation.* **27**, 161-74 (2003). https://doi.org/10.1023/a:1025076111950
78. Lee, H. S.; Park, J. H.; Kang, J. H.; Kawada, T.; Yu, R.; Han, I. S. Chemokine and chemokine receptor gene expression in the mesenteric adipose tissue of KKAy mice. *Cytokine.* **46**, 160-5. (2009). https://doi.org/10.1016/j.cyto.2008.12.025
79. Marinkovic, T.; et al. Interaction of mature $CD3^{+}CD4^{+}$ T cells with dendritic cells triggers the development of tertiary lymphoid structures in the thyroid. *J. Clin. Invest.* **116**, 2622-32 (2006). https://doi.org/10.1172/jci28993
80. Makuch, E.; Jasyk, I.; Kula, A.; Lipiński, T.; Siednienko, J. IFNβ-induced CXCL10 chemokine expression is regulated by pellino3 ligase in monocytes and macrophages. International journal of molecular sciences. **23**, 14915 (2022). https://doi.org/10.3390/ijms232314915
81. Liu, P. P.; et al. Neuronal cathepsin S increases neuroinflammation and causes cognitive decline via CX3CL1-CX3CR1 axis and JAK2-STAT3 pathway in aging and Alzheimer's disease. *Aging Cell.* **24**, e14393 (2025). https://doi.org/10.1111/acel.14393

CORE ★ AUTHORS

Fudi Wang is the Qiushi Distinguished Professor at Zhejiang University. Recognized globally as the founding pioneer of the field of Ferrology and a leading authority on ferroptosis, he has received the National Outstanding Youth Fund, been inducted into the National Ten-Thousand Talents Program, and serves as the Chief Scientist for national key R&D programs. He is also a recipient of the State Council Special Allowance. Prof. Wang's seminal contributions have established the core theoretical framework of ferroptosis signaling and pioneered the systemic investigation of metal homeostasis. He has introduced the transformative concepts of ferrolipid, ferroplasticity, and ferro-guardian, while systematically identifying novel genes, core regulatory pathways, and clinically translatable therapeutic targets. He holds dual Clarivate and Elsevier Highly Cited Researcher distinctions and consistently ranks among the world's top 2% of scientists (h-index 85; >29,400 citations). He has authored nearly 280 high-impact publications in journals including *Cell*, *Nature*, and *Cell Metabolism*, with a cumulative impact factor exceeding 3500 and 31 cover-story selections. In addition to his research, Prof. Wang serves as Editor-in-Chief of *Element*, Deputy Editor of *Research*, and an Editorial Board member for *Cell Metabolism*. He has held multiple senior leadership positions—including President, Vice President, and Dean—across various universities and institutes, with extensive oversight of education and academic administration.

Junxia Min is a Full Professor and Doctoral Supervisor with a joint appointment at the Institute of Translational Medicine and The First Affiliated Hospital, Zhejiang University School of Medicine. She also serves as President of the Trace Element Branch of the Biophysical Society of China. As a recipient of the Elsevier Highly Cited Chinese Researcher award, her translational research program is centered on three interconnected pillars: ferroptosis signaling in major human diseases, the development of novel anti-tumor therapeutics, and the molecular mechanisms governing aging and longevity. By integrating long-term human population cohorts, genetically engineered murine models, and multi-omics profiling platforms, her team systematically dissects disease pathogenesis and translates these insights into clinical applications. Prof. Min has authored over 140 high-impact publications in leading journals, including *Cell, Nature, Nature Medicine, Cell Metabolism*, and *Nature Reviews Cardiology* and *Nature Reviews Immunology*. Her seminal work includes the identification of human longevity-related genes and mechanisms, establishes solid theoretical frameworks and builds clinically actionable pipelines targeting ferroptosis for disease prevention, targeted cancer treatment, and the promotion of human healthspan.

Guenter Weiss, MD studied medicine at the University of Innsbruck, Austria, and performed a thesis at the Institute for Medical Chemistry and Biochemistry. He then worked as a post-doctoral fellow at the Department of Medical Chemistry and Biochemistry before starting as a resident at the Department of Internal Medicine at the University of Innsbruck, where he did his medical training in internal medicine. He became a specialist in internal medicine in 1998, in intensive care medicine in 2001, and in infectious diseases in 2006. His clinical training was interrupted by another post-doctoral fellowship at the EMBL in Heidelberg where he worked on translational gene regulation (until 1996). Thereafter, he built up his own research group supported by grants from

the Austrian Research Funds, the European Union, and the National Institute of Health. Dr. Weiss successfully completed two habilitations (Medical Biochemistry in 1995, Internal Medicine in 1999) and still tries to combine his daily clinical work and duties with scientific laboratory and clinically based projects. Guenter Weiss has published more than 450 papers in peer-reviewed journals (h-index 118). His research focuses on multiple aspects of cellular and systemic iron homeostasis and their dysregulation in specific pathological conditions including anemia of chronic diseases and iron overload. Furthermore, he studies the regulatory network between metabolism, immune function, and infection, with a specific emphasis on the role of macrophages in host-pathogen interaction and the impact of natural resistance genes and metabolic alterations in the host-pathogen micro-environment on disease outcome. Since 2012, Guenter Weiss has been a full professor of medicine at the Medical University of Innsbruck and director of the Division of Internal Medicine II (infectious diseases, immunology, rheumatology, pneumology). In 2015, he was elected into the Austrian Academy of Science, and in 2022 into the Academia Europaea - European Academy of Science.

Liyun Chen was a postdoctoral fellow in the laboratories of Drs. Wang and Min. He is currently a researcher at the Binjiang Institute of Zhejiang University. He obtained his Ph.D. in Nutrition and Food Hygiene from Zhejiang University (Hangzhou, China) and completed his postdoctoral training at Zhejiang University (Hangzhou, China). During his doctoral and postdoctoral studies, he focused on the functions and mechanisms of trace elements in the hematopoietic and immune systems. His research papers have been published as first author in internationally renowned journals, including *Signal Transduction and Targeted Therapy, Science Bulletin,* and *Advances in Nutrition.*

Wenxi Zhao was a master's student in Dr. Wang's laboratory. She currently works as a staff member at the Department of Nutrition, Peking University Hospital of Stomatology (Beijing, China). She received her Bachelor's degree in Food Hygiene and Nutrition from Chongqing Medical University (Chongqing, China), and her Master's degree from Zhejiang University School of Public Health (Hangzhou, China). In 2026, she joined the Department of Nutrition at Peking University Hospital of Stomatology. During her master's training, she participated in three research projects and contributed as a coauthor (including as cofirst author and as seventh author) on related publications.

Qian Wu is an Associate Professor at Global Innovation Institute of Element Science (GIIES-JLU), The First Hospital of Jilin University in Changchun, China. He received his Ph.D. in Biochemistry and Molecular Biology from Chinese Academy of Sciences (Shanghai, China) and completed postdoctoral training at Zhejiang University (Hangzhou, China). In 2026, he joined The First Hospital of Jilin University, where he established the Metal Immunity Laboratory at Institute of Elemental Science. As principal investigator, he is funded by the National Natural Science Foundation of China, including grants from the General Program and the Young Scientists Fund in the Life Sciences Division. His research on metal metabolism has been published as first and/or corresponding author in leading international journals, including *Science Immunology, EMBO Journal*, and *Cell Metabolism*.